

國立交通大學

電信工程學系

碩士論文

正交分頻多工系統中用於通道估計之  
新型路徑選取方法



A Novel Path Selection Method for  
Channel Estimation in OFDM Systems

研究生：杜欣憶

指導教授：黃家齊 博士

中華民國九十六年七月

正交分頻多工系統中用於通道估計之  
新型路徑選取方法

A Novel Path Selection Method for  
Channel Estimation in OFDM Systems

研究生：杜欣憶

Student : Hsin-Yi Tu

指導教授：黃家齊

Advisor : Dr. Chia-Chi Huang

國立交通大學

電信工程學系碩士班



A Thesis

Submitted to Department of Communication Engineering  
College of Electrical and Computer Engineering  
National Chiao Tung University  
in Partial Fulfillment of the Requirements  
for the Degree of  
Master of Science  
in  
Communication Engineering  
July 2007  
Hsinchu, Taiwan, Republic of China

中華民國九十六年七月

# 正交分頻多工系統中用於通道估計之 新型路徑選取方法

學生：杜欣憶

指導教授：黃家齊

國立交通大學電信工程學系 碩士班



本論文提出一種運用於正交分頻多工系統中通道估計之新型路徑選取方法。此方法所形成的成本函數可視為一整數線性規劃問題，並且我們發現這個問題可再被簡化為一個排序問題，我們更進一步地藉由誤判、漏判事件以及訊號對雜訊與通道估計錯誤比的分析來設定新的臨界值以進一步改良此方法。模擬結果顯示，相較於二種簡單傳統路徑選取方法，我們提出的方法可以改善位元錯誤率，減少通道估計的平方誤差，並增加選擇到正確通道路徑的機率。最後，從模擬結果亦可以發現我們所提出的方法對於多重路徑的功率延遲及所操作的訊號雜訊比並不敏感。

# A Novel Path Selection Method for Channel Estimation in OFDM Systems

Student : Hsin-Yi Tu

Advisor : Dr. Chia-Chi Huang

Department of Communication Engineering  
National Chiao Tung University

## ABSTRACT

In this thesis, we propose a novel path selection method for channel estimation in OFDM systems. The formulated cost function of the proposed method can first be looked upon as an integer linear programming (ILP) problem. We then find that the ILP problem can be further simplified into a sorting problem. In order to refine the proposed algorithm, we further set a new threshold for the algorithm by analyzing the event of false alarm and miss detection and signal to noise and estimation error ratio. Comparing to the two simple conventional methods, our simulation results show that the proposed method can improve bit error rate (BER) performance, reduce square error (SE) of channel estimation, and increase the probability of correctly selecting channel paths. Finally, our simulation results also show that the proposed method is insensitive to the multipath power delay profile as well as the operating signal-to-noise ratio (SNR).

## 誌 謝

首先感謝黃家齊教授對於我生活、學業上的指導，還有對於論文內容的建議。也謝謝口試委員吳文榕和陳紹基教授給予本論文的指教，使我的論文更臻完善。

特別感謝古孟霖學長在我碩士班就讀期間，對於我學業上的問題，不厭其煩地教導。此外，也給我論文製作的方向，即使再忙，仍願意抽空跟我討論，甚至在我為論文進度心煩氣躁時，都一直給我最大的鼓勵。如果沒有學長，就不會有這本論文的完成。

謝謝實驗室學長姐一直以來對我的照顧：Amy、肖真、香君，還有常給我便利商店點數的旺旺，也謝謝同屆同學的相互砥礪和協助。

謝謝一起提前入學的勝文和阿傑：勝文陪我打球，在我心情不好時安慰我；阿傑則是和我互相到對方實驗室串門子。謝謝室友惠婷和小天的陪伴，讓我不覺得孤單。

我要感謝我的爸爸、媽媽和哥哥。你們除了給我物質上的支持，讓我不感匱乏，也是我情感上最強大的後盾。你們是我最重要的家人。

最後，僅以本論文，獻給我愛的爺爺和奶奶，希望你們在天上也能以我為傲。

# Contents

<b>Chapter 1 Introduction .....</b>	<b>1</b>
<b>Chapter 2 OFDM System.....</b>	<b>5</b>
2.1 System Model .....	6
2.2 DFT Implementation for OFDM Systems.....	8
2.3 Orthogonality.....	10
2.4 Guard Interval.....	12
2.5 The Pros and Cons of OFDM System .....	14
<b>Chapter 3 DFT-Based Channel Estimation.....</b>	<b>16</b>
3.1 Signal Model .....	18
3.2 Maximum Likelihood Estimator .....	19
<b>Chapter 4 Conventional Path Selection Methods.....</b>	<b>22</b>
4.1 Threshold Setting Method .....	23
4.2 Number of Path Setting Method.....	24
<b>Chapter 5 Proposed Path Selection Method .....</b>	<b>26</b>
5.1 Cost Function.....	28
5.2 Optimum Solution .....	31
5.3 Refined Path Selection Method .....	32
5.3.1 Analysis of False Alarm .....	33
5.3.2 Algorithm .....	34
5.3.3 Determination of the Parameter U.....	35
<b>Chapter 6 Simulation Results.....</b>	<b>41</b>
6.1 Threshold for Refined Path Selection Method .....	44
6.2 System Performance in Veh. A Channel .....	52
6.3 System Performance in Veh. B Channel.....	58
6.4 System Performance in two-path Channel .....	63
6.5 System Performance in thirty-path Channel.....	69
6.5.1 System Performance of Number of Path Setting Method with Different $N_p$ .....	75
<b>Chapter 7 Conclusions .....</b>	<b>77</b>

**Bibliography .....79**



# List of Tables

Table 5.1 The probability of false alarm and miss detection with $U$ as a parameter.....	39
Table 6.1 Simulation parameters .....	41
Table 6.2 Power delay profiles of channel environments.....	42





# List of Figures

Figure 2.1 (a) Transmitter of a multi-carrier system and (b) receiver of a multi-carrier system.....	6
Figure 2.2 An arrangement for subcarriers that avoids the ICI but occupies too large.....	8
Figure 2.3 An arrangement for subcarriers that avoids the ICI and save a lot of bandwidth.....	8
Figure 2.4 FFT implementation for an OFDM system.....	9
Figure 2.5 Spectrum of mutual orthogonal subcarriers. ....	12
Figure 2.6 Effect of multipath with silent guard interval in an OFDM system; the delayed sucarrrier 2 causes ICI on subcarrier 1, and vice versa.....	13
Figure 2.7 Complete OFDM symbol; $N_g$ is the length of CP and $N$ is the length of useful symbol.....	14
Figure 3.1 The block diagram of the DFT-based channel estimation method.....	17
Figure 4.1 The block diagram of the DFT-based channel estimation method with path.....	22
Figure 6.1 The BER performance for the proposed path selection method in the Veh. A channel at $E_b/N_0 = 10\text{dB}$ with threshold as a parameter. ....	46
Figure 6.2 The average SE for the proposed path selection method in the Veh. A channel at $E_b/N_0 = 10\text{dB}$ with threshold as a parameter. ....	46
Figure 6.3 The BER performance for the proposed path selection method in the Veh. A channel at $E_b/N_0 = 40\text{dB}$ with threshold as a parameter. ....	47
Figure 6.4 The average SE for the proposed path selection method in the Veh. A channel at $E_b/N_0 = 40\text{dB}$ with threshold as a parameter. ....	47
Figure 6.5 The BER performance for the proposed path selection method in the thirty-path channel at $E_b/N_0 = 10\text{dB}$ with threshold as a parameter. ....	48
Figure 6.6 The average SE for the proposed path selection method in the thirty-path channel at $E_b/N_0 = 10\text{dB}$ with threshold as a parameter. ....	48
Figure 6.7 The BER performance for the proposed path selection method in the thirty-path channel at $E_b/N_0 = 40\text{dB}$ with threshold as a parameter. ....	49
Figure 6.8 The average SE for the proposed path selection method in the thirty-path channel at $E_b/N_0 = 40\text{dB}$ with threshold as a parameter. ....	49
Figure 6.9 The BER performance for the proposed path selection method in the two-path channel at $E_b/N_0 = 10\text{dB}$ with threshold as a parameter. ....	50
Figure 6.10 The average SE for the proposed path selection method in the two-path channel at $E_b/N_0 = 10\text{dB}$ with threshold as a parameter. ....	50

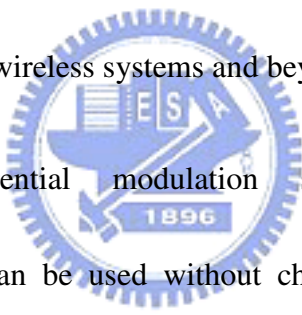
Figure 6.11 The BER performance for the proposed path selection method in the two-path channel at $E_b/N_0 = 40\text{dB}$ with threshold as a parameter. ....	51
Figure 6.12 The average SE for the proposed path selection method in the two-path channel at $E_b/N_0 = 40\text{dB}$ with threshold as a parameter. ....	51
Figure 6.13 The BER performance for the three path selection methods in the Veh. A channel.....	54
Figure 6.14 The average SE for the three path selection methods in the Veh. A channel. ....	54
Figure 6.15 The CDF of false alarm for the three path selection methods at $E_b/N_0 = 10\text{dB}$ in the Veh. A channel. ....	55
Figure 6.16 The CDF of miss detection for the three path selection methods at $E_b/N_0 = 10\text{dB}$ in the Veh. A channel. ....	55
Figure 6.17 The CDF of false alarm for the three path selection methods at $E_b/N_0 = 25\text{dB}$ in the Veh. A channel. ....	56
Figure 6.18 The CDF of miss detection for the three path selection methods at $E_b/N_0 = 25\text{dB}$ in the Veh. A channel. ....	56
Figure 6.19 The CDF of false alarm for the three path selection methods at $E_b/N_0 = 40\text{dB}$ in the Veh. A channel. ....	57
Figure 6.20 The CDF of miss detection for the three path selection methods at $E_b/N_0 = 40\text{dB}$ in the Veh. A channel. ....	57
Figure 6.21 The BER performance for the three path selection methods in the Veh. B channel.....	59
Figure 6.22 The average SE for the three path selection methods in the Veh. B channel. ....	59
Figure 6.23 The CDF of false alarm for the three path selection methods at $E_b/N_0 = 10\text{dB}$ in the Veh. B channel. ....	60
Figure 6.24 The CDF of miss detection for the three path selection methods at $E_b/N_0 = 10\text{dB}$ in the Veh. B channel. ....	60
Figure 6.25 The CDF of false alarm for the three path selection methods at $E_b/N_0 = 25\text{dB}$ in the Veh. B channel. ....	61
Figure 6.26 The CDF of miss detection for the three path selection methods at $E_b/N_0 = 25\text{dB}$ in the Veh. B channel. ....	61
Figure 6.27 The CDF of false alarm for the three path selection methods at $E_b/N_0 = 40\text{dB}$ in the Veh. B channel. ....	62
Figure 6.28 The CDF of miss detection for the three path selection methods at $E_b/N_0 = 40\text{dB}$ in the Veh. B channel. ....	62
Figure 6.29 The BER performance for the three path selection methods in the two-path channel.....	65
Figure 6.30 The average SE for the three path selection methods in the two-path channel.....	65

Figure 6.31 The CDF of the false alarm for the three path selection methods at $E_b/N_0 = 10\text{dB}$ in the two-path channel.....	66
Figure 6.32 The CDF of miss detection for the three path selection methods at $E_b/N_0 = 10\text{dB}$ in the two-path channel.....	66
Figure 6.33 The CDF of the false alarm for the three path selection methods at $E_b/N_0 = 25\text{dB}$ in the two-path channel.....	67
Figure 6.34 The CDF of miss detection for the three path selection methods at $E_b/N_0 = 25\text{dB}$ in the two-path channel.....	67
Figure 6.35 The CDF of the false alarm for the three path selection methods at $E_b/N_0 = 40\text{dB}$ in the two-path channel.....	68
Figure 6.36 The CDF of miss detection for the three path selection methods at $E_b/N_0 = 40\text{dB}$ in the two-path channel.....	68
Figure 6.37 The BER performance for the three path selection methods in the thirty-path channel.....	71
Figure 6.38 The average SE performance for the three path selection methods in the thirty-path channel.....	71
Figure 6.39 The CDF of false alarm for the three path selection methods at $E_b/N_0 = 10\text{dB}$ in the thirty-path channel.....	72
Figure 6.40 The CDF of miss detection for the three path selection methods at $E_b/N_0 = 10\text{dB}$ in the thirty-path channel.....	72
Figure 6.41 The CDF of false alarm for the three path selection methods at $E_b/N_0 = 25\text{dB}$ in the thirty-path channel.....	73
Figure 6.42 The CDF of miss detection for the three path selection methods at $E_b/N_0 = 25\text{dB}$ in the thirty-path channel.....	73
Figure 6.43 The CDF of false alarm for the three path selection methods at $E_b/N_0 = 40\text{dB}$ in the thirty-path channel.....	74
Figure 6.44 The CDF of miss detection for the three path selection methods at $E_b/N_0 = 40\text{dB}$ in the thirty-path channel.....	74
Figure 6.45 The BER performance for the number of path setting method with $N_p$ as a parameter in the thirty-path channel.....	76
Figure 6.46 The average SE for the number of path setting method with $N_p$ as a parameter in the thirty-path channel.....	76

# Chapter 1

## Introduction

Orthogonal frequency division multiplexing (OFDM) has received considerable interest in recent years. Due to its advantages in high-data-rate transmissions over frequency-selective fading channels and ability to provide a substantial reduction in equalization complexity compared to classical modulation techniques [1] [2], OFDM is used for high-data-rate wireless local area network (WLAN) standards, such as ETSI Hiperlan II and IEEE 802.11a, providing data rates up to 54Mbps/s, and considered for the fourth-generation (4G) mobile wireless systems and beyond [3].

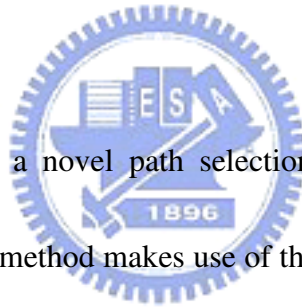


Although some differential modulation schemes such as differential phase-shift-keying (DPSK) can be used without channel state information [4], these differential modulation schemes degrade system performance in signal-to-noise ratio (SNR) as compared with non-differential modulation schemes such as quadrature phase-shift-keying (QPSK). In general, non-differential modulation schemes require channel state information for coherent demodulation at the receiver side. In spite of the fact that some blind techniques that exploit statistical or deterministic properties of the transmitted and received signals are developed, their applications are only limited in phase-shift-keying (PSK) modulation. For multilevel modulation schemes with nonconstant envelope, like quadrature amplitude modulation (QAM), coherent

demodulation that needs to estimate and track parameters of fading channel is still needed [1]. Therefore, channel estimation is an essential issue for implementing a successful OFDM system.

A number of algorithms have been presented for channel estimation in OFDM systems. One of them uses Discrete Fourier transform (DFT) to perform channel estimation and this method is called DFT-based channel estimation. The DFT-based channel estimation method, derived from either maximum likelihood (ML) criterion or minimum mean square error (MMSE), was originally proposed for single-input single-output (SISO)/OFDM systems with pilot preambles. This method is composed of a least square (LS) estimator, an inverse DFT (IDFT) matrix, a weighting matrix, and a DFT matrix [1] [2] [5]. The LS estimator exploits pilot symbols to produce an LS estimate, which is a noisy observation of channel frequency response. After taking the IDFT to transform the estimate to time domain, we can improve this estimate by using a weighting matrix which depends on the performance criterion used (MMSE or ML criterion). Note that when equally spaced pilot symbols are used, the weighting matrix degenerates into an identity matrix. Finally, the enhanced estimate is transformed back to frequency domain to obtain a new estimate of channel frequency response. To further improve the DFT-based channel estimation method, we can utilize a path selection method to reserve desired channel paths and to suppress noise.

The robustness of path selection has great influence on the system performance and the complexity of channel tracking. There are two conventional path selection methods: number of path setting method and threshold setting method [6] [7]. For these two methods, if the value of the desired number of total paths (a parameter in the number of path setting method) or the value of the threshold (a parameter in the threshold setting method) are set too large, the ability to suppress noise in the path selection method is reduced, thereby lowering the improvement of system performance and increasing the complexity of channel tracking. On the other hand, if these two values are set too small, true channel paths are excluded and the system performance degrades. As a result, it is difficult to set proper values of these two parameters for the two conventional path selection methods, since the setting of the parameters are sensitive to channel environments.



In this thesis, we propose a novel path selection method for channel estimation in OFDM systems. The proposed method makes use of the linear programming method to find an optimum solution which selects channel paths more precisely and less sensitively to the parameters. We first form a cost function for the proposed path selection method and then this cost function can be represented as an integer linear programming problem (ILP). Moreover, since the variables involved are binary, we can finally simplify this problem as a sorting problem. In addition, a threshold which is insensitive to channel conditions (e.g., power delay profiles) is introduced to refine the proposed path selection method.

The rest of this paper is organized as follows. Chapter 2 describes an OFDM system and addresses the feature of the system. Chapter 3 introduces a DFT-based channel estimation

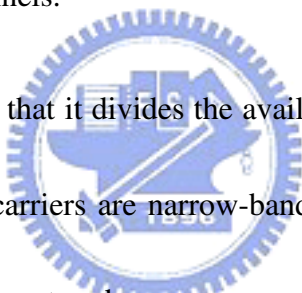
method derived from ML criterion. Chapter 4 presents two conventional time domain path selection methods: the number of path setting method and the threshold setting method. Chapter 5 proposes a novel path selection method which is less sensitive to parameters and channel conditions than the two conventional methods. The performance of the proposed method is then evaluated in Chapter 6. Finally, some conclusions and future works are drawn in the last chapter.



# Chapter 2

## OFDM System

OFDM, which was brought up in the mid 60's, is a digital multi-carrier modulation scheme. In recent years, it has been adopted for many applications in wireless communication systems, such as WLAN and digital video broadcasting (DVB) [2], as a result of its capability of high-rate transmission and low-complexity implementation over frequency-selective fading channels.



The basic idea of OFDM is that it divides the available spectrum into several orthogonal subcarriers. Because these subcarriers are narrow-band, they experience flat fading channel and equalization method of the system becomes very simple. Furthermore, it possesses high spectral efficiency by overlapping these orthogonal subcarriers [8]. Moreover, the insertion of cyclic prefix (CP), which preserves the periodic extensions of the transmitted signal, can eliminate intersymbol and intercarrier interference caused by multipath environments.

This chapter gives a description of the principle and feature of an OFDM system.



## 2.1 System Model

An OFDM system is a kind of multi-carrier modulation schemes. It splits a high-rate bit stream into a number of low-rate bit streams. These low-rate bit streams are modulated onto different subcarriers and transmitted simultaneously [9]. The increase in symbol duration due to the narrowband subcarriers makes the amount of multipath delays relatively small and lets the OFDM system easily implemented in frequency-selective fading channels.

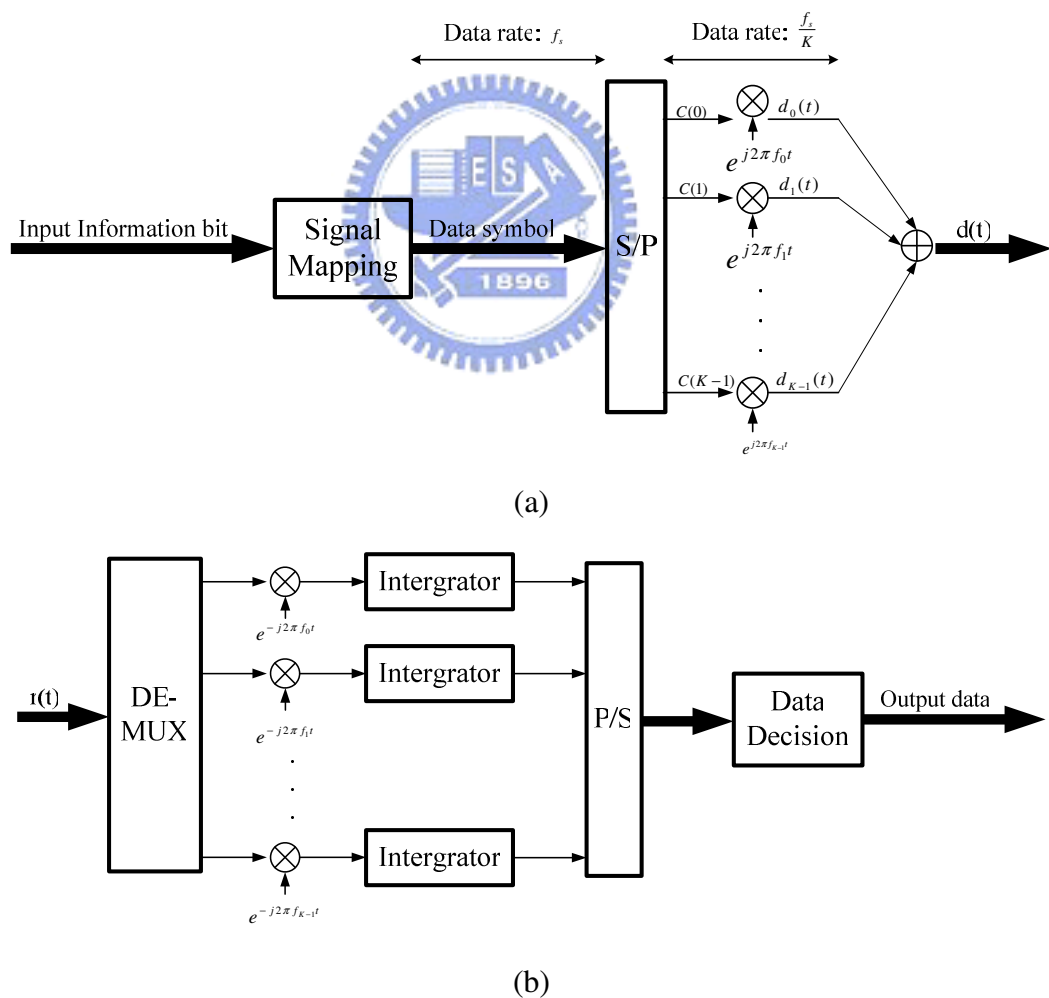


Figure 2.1 (a) Transmitter of a multi-carrier system and (b) receiver of a multi-carrier system

Figure 2.1 (a) and (b) are the transmitter and the receiver of a multi-carrier system, respectively. After serial-to-parallel (S/P) converter, all data streams are modulated onto subcarriers simultaneously. Data rate of these parallel streams becomes  $f_s / K$ , where the data rate of the original data stream is  $f_s$ . Thus the system is more resistant to the effect of intersymbol interference (ISI).

The signal on the  $k$ th subcarrier can be represented by

$$d_k(t) = c(k)e^{j2\pi f_k t} \quad (2.1)$$

where  $c(k)$  is the modulated data symbol,  $f_k$  is the carrier frequency of the  $k$ th subcarrier, and  $t$  is the time index.

The output of the transmitter is a juxtaposition of individual signal of each subcarrier:

$$d(t) = \sum_{k=0}^{K-1} c(k)e^{j2\pi f_k t} \quad (2.2)$$

It needs to choose  $K$  proper frequencies, i.e.  $f_0, f_1, \dots, f_{K-1}$ , to avoid intercarrier interference (ICI) among subcarriers. Figure 2.2 provides a kind of arrangement for subcarriers. Although this arrangement meets the purpose of no ICI among the subcarriers, it occupies too large bandwidth. On the other hand, the arrangement of the orthogonal subcarriers shown in Figure 2.3 can not only avoid the ICI among subcarriers, but also save a lot of bandwidth.

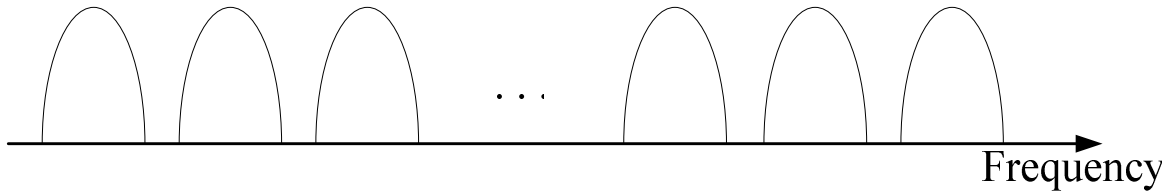


Figure 2.2 An arrangement for subcarriers that avoids the ICI but occupies too large bandwidth.

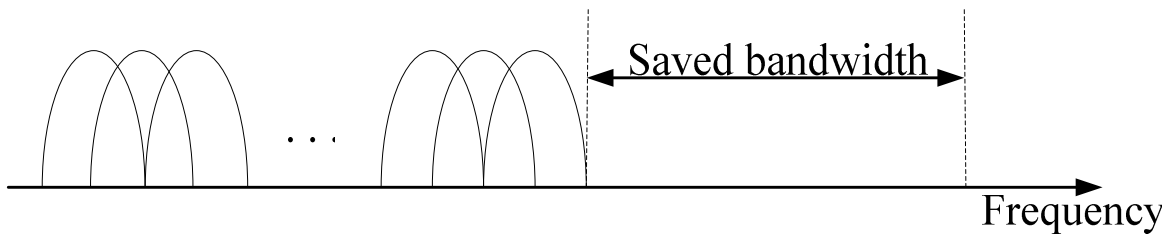


Figure 2.3 An arrangement for subcarriers that avoids the ICI and save a lot of bandwidth.

## 2.2 DFT Implementation for OFDM Systems



A system shown in Figure 2.1 needs  $K$  oscillators to generate  $K$  orthogonal subcarriers.

We can introduce a DFT operation as an alternative to make the implementation much easier.

The OFDM signals by using the operation of DFT are generated as follows. By sampling Eq.(2.2) with sampling rate  $1/T_s$ , we can obtain

$$d(nT_s) = \sum_{k=0}^{K-1} c(k)e^{j2\pi f_k nT_s}. \quad (2.3)$$

If we have  $f_k = k / KT_s$ , Eq.(2.3) can be rewritten in a discrete form as follows

$$d[n] = \sum_{k=0}^{K-1} c(k) e^{j2\pi \frac{kn}{K}}. \quad (2.4)$$

According to the formula of the IDFT

$$b[n] = \sum_{k=0}^{K-1} B[k] e^{j2\pi \frac{kn}{K}}, \quad (2.5)$$

we get

$$d[n] = IDFT\{c(k)\}. \quad (2.6)$$

Consequently, the DFT operation can be applied to an OFDM system. In addition, when  $K$  is equal to  $2^m$  ( $m$  is a positive integer), the fast Fourier transform (FFT) operation can be used for faster implementation in an OFDM system, as shown in Figure 2.4.

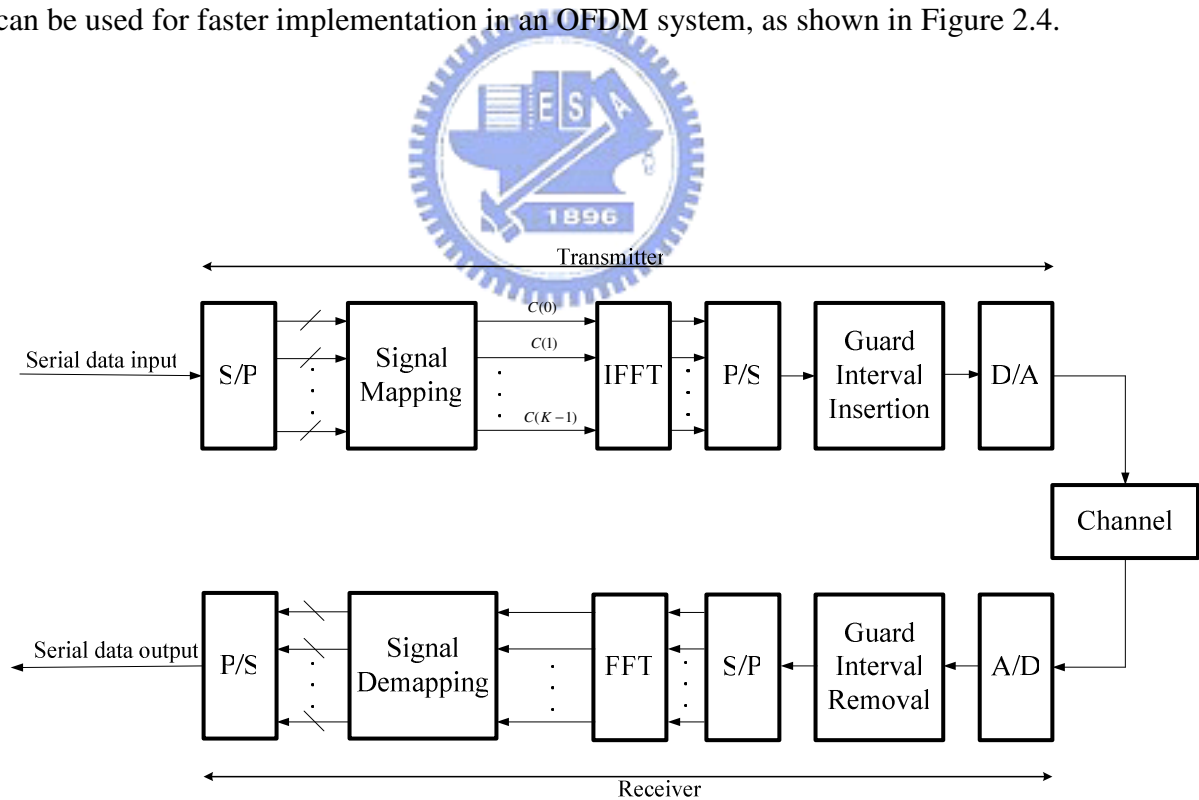
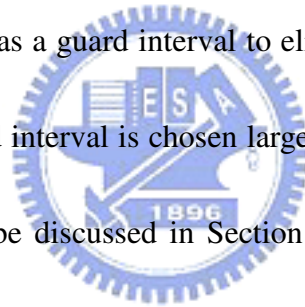


Figure 2.4 FFT implementation for an OFDM system.

In Figure 2.4, we consider an OFDM system employing  $K$  subcarriers for transmission. After the S/P converter, a serial high-rate bit stream is partitioned into  $K$  parallel low-rate streams which are then mapped into symbols by using a modulation constellation scheme, such as QAM and PSK. Each of the  $K$  modulated data symbols  $c(k)$ , for  $k=0, \dots, K-1$ , is mapped from several bits by using the corresponding modulation scheme. These symbols are fed to a  $K$ -point IDFT unit to generate time-domain samples. The parallel time-domain samples are then converted into serial ones by using the parallel-to-serial (P/S) converter. Afterwards, a cyclic prefix is inserted in front of these time-domain samples as a guard interval to eliminate ISI between adjacent OFDM symbols. The length of a guard interval is chosen larger than the delay spread. More details about the guard interval will be discussed in Section 2.4. Finally, the OFDM symbols is passed through a digital-to-analog converter (DAC) and transmitted in air. The receiver in Figure 2.4 behaves as inverse operation of the transmitter.



## 2.3 Orthogonality

Unlike the conventional frequency division multiplexing (FDM) systems, orthogonality among subcarriers greatly simplifies the design of both the transmitter and the receiver. Due to the orthogonality, a simplified one-tap equalizer can be used for each subcarrier. The

orthogonality allows high spectral efficiency as well, and almost the whole available frequency band can be utilized.

For an OFDM system, we can use the DFT operation to produce the subcarriers which are orthogonal to each other. We show this feature in the following. Assume that subcarriers are of the form:

$$\varphi_k(t) = e^{j2\pi f_k t}, \quad k = 0, 1, \dots, K-1 \quad (2.7)$$

where  $f_k = k / KT_s$  and  $T_s$  is a sampling period. For the  $k_1$ th and the  $k_2$ th subcarriers, we have

$$\begin{aligned} & \int_a^b (e^{j2\pi \frac{k_1}{KT_s} t})(e^{j2\pi \frac{k_2}{KT_s} t})^* dt \\ &= \int_a^b (e^{j2\pi \frac{(k_1-k_2)}{KT_s} t}) dt \\ &= \frac{e^{j2\pi(k_1-k_2)\frac{b}{KT_s}} [1 - e^{j2\pi(k_1-k_2)\frac{(a-b)}{KT_s}}]}{j2\pi(k_1-k_2)\frac{1}{KT_s}} \\ &= \begin{cases} (b-a) & \text{for } k_1 = k_2 \\ 0 & \text{for } k_1 \neq k_2 \text{ and } (b-a) = KT_s \end{cases} \end{aligned} \quad (2.8)$$

As can be seen in Eq. (2.7) and Eq(2.8), when the subcarrier frequencies  $f_k$  are chosen as integer multiples of  $1/KT_s$ , they will be orthogonal to each other for an integration interval  $KT_s$ .

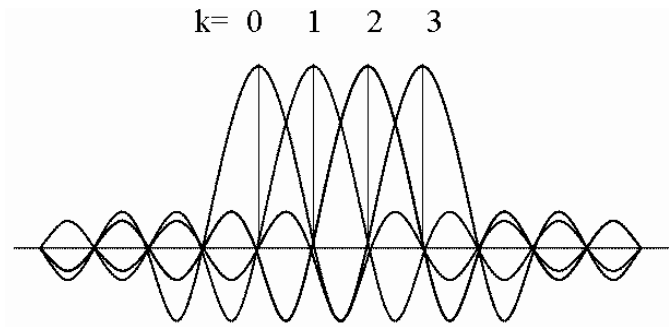


Figure 2.5 Spectrum of mutual orthogonal subcarriers.

Moreover, as shown in Figure 2.5, if we sample at the peak of each subcarrier, there will be no ICI among these subcarriers.

## 2.4 Guard Interval

One of the most important feature for an OFDM system is its efficient way to handle multipath interference. Since the system bandwidth is divided into  $K$  subcarriers, the symbol duration is increased and the ISI caused by a time-dispersive fading environment is mitigated. To eliminate ISI completely, a guard interval is inserted at the beginning of each OFDM symbol. The guard interval is chosen longer than the maximum channel delay spread, in order to avoid multipath components from one OFDM symbol interfering with the next adjacent OFDM symbol.

If a silent guard interval is adopted in an OFDM system, rather than the cyclic prefix, the effect of ICI would arise among subcarriers due to the fact that the orthogonality of

subcarriers is no longer preserved [9]. The effect of ICI is illustrated in Figure 2.6.

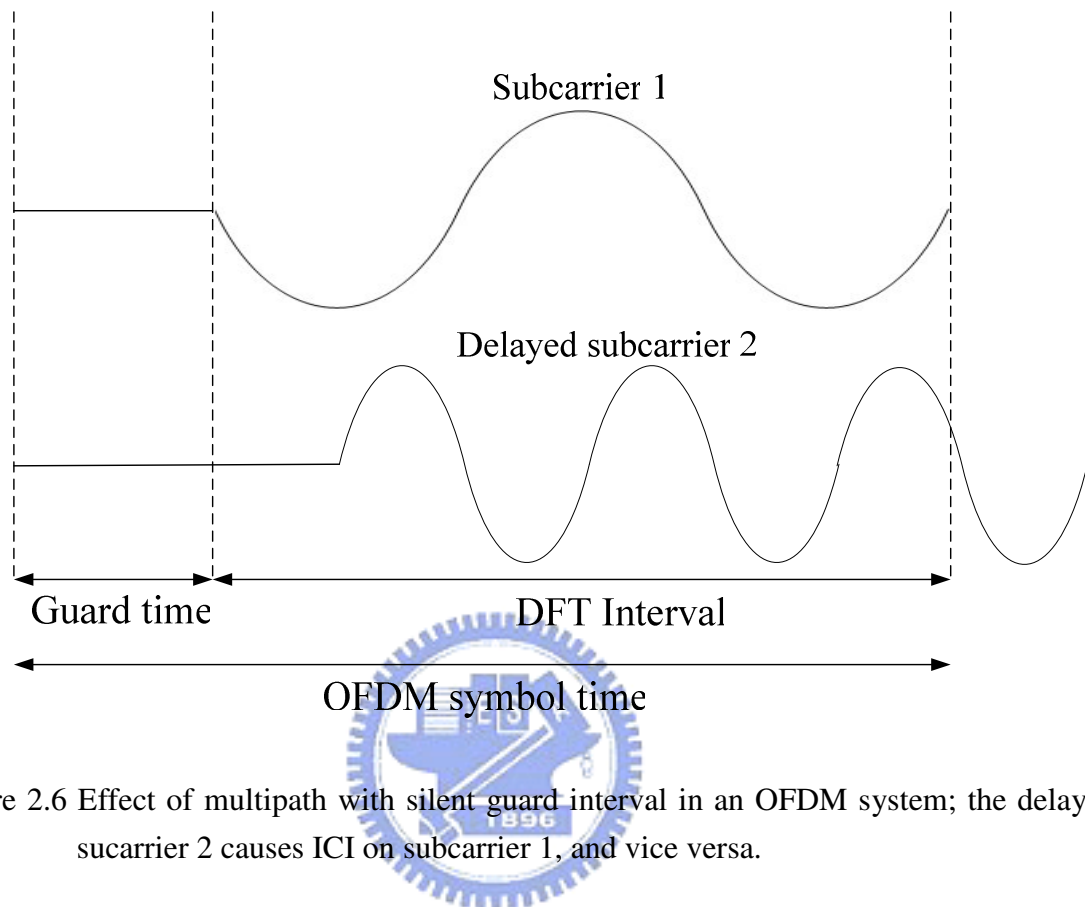


Figure 2.6 Effect of multipath with silent guard interval in an OFDM system; the delayed subcarrier 2 causes ICI on subcarrier 1, and vice versa.

As shown in Figure 2.6, there are two time-domain sinusoids, corresponding to two orthogonal subcarriers in frequency domain, called subcarrier 1 and subcarrier 2, respectively. Due to the multipath delay, the orthogonality between the subcarrier 1 and the subcarrier 2 is destroyed within the DFT interval. When an OFDM receiver tries to demodulate the subcarrier 1, the delayed subcarrier 2 will induce interference to the subcarrier 1.

On the other hand, “cyclic prefix (CP)” is an alternative to eliminate the ICI, and it is



adopted in most OFDM-based wireless communication systems. For this method, the cyclic extension of an OFDM symbol is inserted in front of the OFDM symbol, as show in Figure 2.7. Therefore, as long as the channel delay is smaller than the guard time, there will be no ICI among subcarriers when the FFT operation is performed in the OFDM demodulator, due to the fact that integration over a period of a sinusoid is achievable.

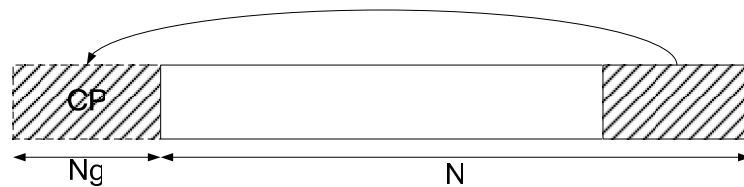
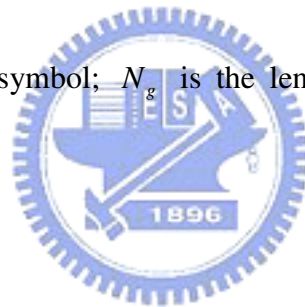


Figure 2.7 Complete OFDM symbol;  $N_g$  is the length of CP and  $N$  is the length of useful symbol.



## 2.5 The Pros and Cons of OFDM System

Since the OFDM system transmits several narrowband signals instead of a wideband signal, a frequency selective fading channel can be transformed into a flat fading channel over each OFDM sub-channel if the sub-channel is sufficiently narrow-banded. As a result, an one-tap equalizer can be applied for OFDM systems, and it is much simpler than the equalizer used for conventional single-carrier modulation systems.

Besides, the longer symbol duration with the insertion of the guard interval makes OFDM systems less sensitive to timing synchronization errors as well as more robust

against the ISI effect, as compared with the single-carrier modulation systems.

In addition, the subcarrier frequencies are chosen so that all subcarriers are orthogonal to each other and therefore the OFDM system can achieve higher spectral efficiency. This orthogonality also permits the use of the FFT operation for the efficient implementation of the modulator and the demodulator in OFDM systems.

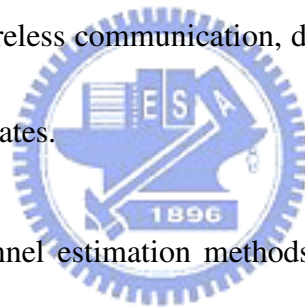
However, there are some disadvantages in the OFDM systems and they are discussed in the following. First of all, because of the orthogonality of subcarriers, the OFDM system is very sensitive to carrier frequency synchronization, and the imperfect frequency synchronization will cause ICI among subcarriers.

Moreover, the OFDM systems usually suffer from the problem of large peak-to-average power ratio, abbreviated as PAPR. This is due to that fact that when  $P$  independent data symbols modulated onto subcarriers within an OFDM symbol are added coherently (with the same phase) in time domain after the IDFT operation, the peak power of the time domain signal is  $P$  times larger than the average power (with the assumption of constant power modulation scheme, e.g. QPSK). For non-constant power modulation scheme, e.g. 16QAM, the PAPR will become much larger. A large PAPR will increase the cost of analog-to-digital and digital-to-analog converters and decrease the power efficiency of power amplifier due to the effect of non-linear distortion.

# Chapter 3

## DFT-Based Channel Estimation

Blind channel estimation, which merely relies on the received signals, is very attractive due to its bandwidth saving advantage. However, it requires a long data record, involves high computational complexity and only applies to slowly time-varying channels. On the contrary, pilot-aided (PA) channel estimation, which uses pilot tones known to the receiver, is widely applied in mobile wireless communication, despite of the fact that the use of pilot tones ends up with lower data rates.



A wide variety of PA channel estimation methods have been proposed. Among these methods, DFT-based channel estimation, derived from either ML criterion or MMSE criterion, for OFDM systems with pilot preambles was intensively investigated. The advantage of the former is simpler to implement, as no information on the channel statistics or the operating signal-to-noise ratio (SNR) is needed in this scheme [1] [2] [5]. On the other hand, DFT-based channel estimation with the MMSE criterion is expected to have better performance as it exploits prior information about the channel statistics and the operating SNR. Furthermore, it has been shown that for DFT-based channel estimation and at intermediate or high SNR values, the performance of an ML estimator is comparable to

that of an MMSE estimator when the number of pilot tones is sufficiently larger than the maximal channel length (in samples) [2].

The DFT-based channel estimation method implemented through four components: a least-square (LS) estimator, an inverse DFT (IDFT) matrix, a weighting matrix, and a DFT matrix, as shown in Figure 3.1.

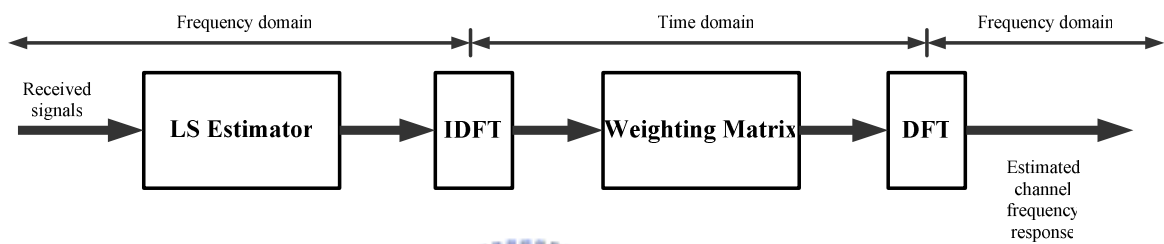


Figure 3.1 The block diagram of the DFT-based channel estimation method



The LS estimate is a noisy observation of channel frequency response. After taking the IDFT operation to transform the estimate to time domain, we can improve this estimate by using a weighting matrix which depends on the performance criterion used. Finally, the enhanced estimate is transformed back to frequency domain to obtain a new estimate of channel frequency response.

### 3.1 Signal Model

We first describe the signal model for the received OFDM symbol as

$$y(n) = h(n) * x(n) + z(n), \quad (3.1)$$

where  $n = 0, \dots, N + G - 1$  is the time index,  $N$  is the total number of subcarriers,  $G$  is the length of guard time,  $y(n)$  is the received OFDM signal,  $x(n)$  is the transmitted pilot signal (including the guard interval),  $h(n)$  is channel impulse response with finite length  $G$ , and  $z(n)$  is additive white Gaussian noise (AWGN) and  $*$  denotes the convolution.

After removing the guard interval and transforming Eq.(3.1) into frequency domain, we

get

$$Y(k) = \sqrt{N}X(k)H(k) + Z(k), \quad (3.2)$$

where  $k$  is the subcarrier index,  $Y(k)$  is the received OFDM signal in frequency domain,  $X(k)$  is the transmitted pilot signal,  $H(k)$  is channel frequency response,  $Z(k)$  is frequency domain AWGN with zero mean and variance  $\sigma_n^2$ ,  $N$  is the total number of subcarriers (or FFT size) and  $\sqrt{N}$  is a FFT normalization factor.

The system model can be rewritten as a vector form:

$$\begin{aligned} \mathbf{Y} &= \sqrt{N}\mathbf{X}\mathbf{H} + \mathbf{Z} \\ &= \sqrt{N}\mathbf{X}\mathbf{F}_h\mathbf{h} + \mathbf{F}_h\mathbf{z}, \end{aligned} \quad (3.3)$$

where  $\mathbf{Y} = [Y(0) \cdots Y(N-1)]^T$  is the received signal vector in frequency domain,  $\mathbf{X}$  is a

diagonal matrix containing the transmitted pilot symbols,  $\{X(0)\cdots X(N-1)\}$ ,  $\mathbf{H}=[H(0),\cdots,H(N-1)]^T$  is the channel impulse response,  $\mathbf{h}=[h(0),\cdots,h(G-1)]^T$  is the channel impulse response with finite length  $G$ ,  $\mathbf{F}_h$  is a truncated DFT matrix of size  $N\times G$ , and  $\mathbf{Z}$  and  $\mathbf{z}$  represent AWGN vector in frequency and time domain respectively and is modeled as independent and identically distributed (i.i.d.) complex Gaussian random vector with zero mean and variance  $\sigma_n^2\mathbf{I}_N$ .

## 3.2 Maximum Likelihood Estimator

The LS estimate for the channel frequency response can be obtained by

$$\hat{\mathbf{H}}_{\text{LS}} = \frac{1}{\sigma_x^2\sqrt{N}}\mathbf{X}^H\mathbf{Y} = \mathbf{F}_h\mathbf{h} + \tilde{\mathbf{Z}}, \quad (3.4)$$

where  $\tilde{\mathbf{Z}} = \frac{1}{\sigma_x^2\sqrt{N}}\mathbf{X}^H\mathbf{Z}$ . By using the LS estimate, we can derive the ML estimate as follows. According to the deterministic model of Eq.(3.4), we would like to find an  $\mathbf{h}$  which maximizes the posteriori probability of  $p(\mathbf{h}|\hat{\mathbf{H}}_{\text{LS}})$ , i.e.,

$$\hat{\mathbf{h}}_{\text{ML}} = \arg \max_{\mathbf{h}} p(\mathbf{h}|\hat{\mathbf{H}}_{\text{LS}}). \quad (3.5)$$

In details, we have

$$p(\mathbf{h}|\hat{\mathbf{H}}_{\text{LS}}) = \frac{p(\hat{\mathbf{H}}_{\text{LS}}|\mathbf{h})p(\mathbf{h})}{p(\hat{\mathbf{H}}_{\text{LS}})}, \quad (3.6)$$

and  $p(\hat{\mathbf{H}}_{LS})$  is a constant value irrelevant to  $\mathbf{h}$ . With the assumption of  $p(\mathbf{h})$  is the same for every  $\mathbf{h}$ , Eq.(3.5) can be rewritten as

$$\begin{aligned}\hat{\mathbf{h}}_{ML} &= \arg \max_{\mathbf{h}} p(\hat{\mathbf{H}}_{LS} | \mathbf{h}) \\ &= \arg \max_{\mathbf{h}} \frac{1}{(\sqrt{2\pi\sigma_n^2})^N} e^{-\frac{\|\hat{\mathbf{H}}_{LS} - \mathbf{F}_h \mathbf{h}\|^2}{2\sigma_n^2}} \\ &= \arg \min_{\mathbf{h}} \|\hat{\mathbf{H}}_{LS} - \mathbf{F}_h \mathbf{h}\|^2.\end{aligned}\quad (3.7)$$

Let  $J(\mathbf{h}) = \|\hat{\mathbf{H}}_{LS} - \mathbf{F}_h \mathbf{h}\|^2$ ,  $J(\mathbf{h})$  can be expanded as a quadratic form

$$\begin{aligned}J(\mathbf{h}) &= \hat{\mathbf{H}}_{LS}^H \hat{\mathbf{H}}_{LS} - 2\hat{\mathbf{H}}_{LS}^H \mathbf{F}_h \mathbf{h} + (\mathbf{F}_h \mathbf{h})^H \mathbf{F}_h \mathbf{h} \\ &= \hat{\mathbf{H}}_{LS}^H \hat{\mathbf{H}}_{LS} - 2\hat{\mathbf{H}}_{LS}^H \mathbf{F}_h \mathbf{h} + \mathbf{h}^H \mathbf{F}_h^H \mathbf{F}_h \mathbf{h}.\end{aligned}\quad (3.8)$$

Making the derivative of  $J(\mathbf{h})$  with respect to  $\mathbf{h}$  be zero, we have

$$\frac{\partial J(\mathbf{h})}{\partial \mathbf{h}} = -2\mathbf{F}_h^H \hat{\mathbf{H}}_{LS} + 2\mathbf{F}_h^H \mathbf{F}_h \mathbf{h} = 0.\quad (3.9)$$

As a result, we obtain the channel estimation corresponding to  $\mathbf{h}$  as follows:

$$\begin{aligned}\hat{\mathbf{h}}_{ML} &= (\mathbf{F}_h^H \mathbf{F}_h)^{-1} \mathbf{F}_h^H \hat{\mathbf{H}}_{LS} \\ &= \mathbf{F}_h^H \hat{\mathbf{H}}_{LS},\end{aligned}\quad (3.10)$$

where  $\mathbf{F}_h^H \mathbf{F}_h = \mathbf{I}_G$ . Substitute Eq.(3.4) into Eq.(3.10), we get

$$\begin{aligned}\hat{\mathbf{h}}_{ML} &= \frac{1}{\sigma_x^2 \sqrt{N}} \mathbf{F}_h^H \mathbf{X}^H \mathbf{Y} \\ &= \mathbf{h} + \frac{1}{\sigma_x^2 \sqrt{N}} \mathbf{F}_h^H \mathbf{X}^H \mathbf{F} \mathbf{z} \\ &= \mathbf{h} + \tilde{\mathbf{z}},\end{aligned}\quad (3.11)$$

where  $\tilde{\mathbf{z}} = \frac{1}{\sigma_x^2 \sqrt{N}} \mathbf{F}_h^H \mathbf{X}^H \mathbf{F} \mathbf{z}$  and the elements of the vector  $\hat{\mathbf{h}}_{ML}$  are denoted as  $\hat{h}_{ML}(n)$ ,

for  $n=0, \dots, G-1$ . As we can see in Eq.(3.11), the ML estimate of channel impulse

response is composed of two components. One is the true channel impulse response and the other is the noise term.





# Chapter 4

## Conventional Path Selection Methods

In order to obtain more accurate channel estimation, we can use path selection methods to suppress the noise in the ML estimate of Eq.(3.11). That is, we pick and reserve significant channel paths by setting the remaining elements in  $\hat{\mathbf{h}}_{\text{ML}}$  as zero.

Figure 4.1 depicts the block diagram of channel estimation with path selection. The LS estimate of channel frequency response is first transformed into time domain to obtain the corresponding channel impulse response. Afterward, the estimate of channel impulse response is passed through a path selection unit to get a refined estimate. This refined estimate is then transformed back into frequency domain to obtain the estimated channel frequency response.

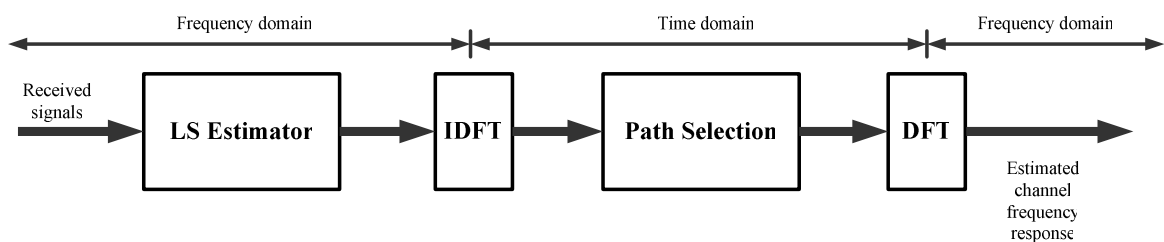


Figure 4.1 The block diagram of the DFT-based channel estimation method with path selection.

This chapter introduces two conventional path selection methods in common use: threshold setting method and number of path setting method. The main strategy of these two conventional path selection methods is to select those elements with larger amplitude (or energy) in  $\hat{\mathbf{h}}_{ML}$  and to suppress noise by setting the remaining elements as zero.

## 4.1 Threshold Setting Method

In the threshold setting method, we first define a threshold and the maximum energy of the ML estimate of channel impulse response  $\hat{\mathbf{h}}_{ML}$  as  $T_{dB}$  and  $\max\left\{\left|\hat{h}_{ML}(n)\right|^2\right\}$ , respectively. In order to select main paths, we reserve those elements in  $\hat{\mathbf{h}}_{ML}$  whose energy (in dB scale) is larger than the value of  $\max\left\{\left|\hat{h}_{ML}(n)\right|^2\right\}_{dB} - T_{dB}$ , where  $\max\left\{\left|\hat{h}_{ML}(n)\right|^2\right\}_{dB}$  is in dB scale, and then discard all the remaining elements by setting their values of  $\hat{h}_{ML}(n)$  as zero. The algorithm of the threshold setting method is presented as follows.

Denote  $T_L$  as the linear scale of  $T_{dB}$ , i.e.,

$$T_L = 10^{\frac{T_{dB}}{10}}. \quad (4.1)$$

Then we can express the estimated channel impulse response with path selection as

$$\hat{h}_{th}(n) = \begin{cases} \hat{h}_{ML}(n), & \text{if } \left|\hat{h}_{ML}(n)\right|^2 \geq \max\left\{\left|\hat{h}_{ML}(n)\right|^2\right\}/T_L, \\ 0, & \text{otherwise} \end{cases}, \quad (4.2)$$

for  $n = 0, \dots, G-1$ .

For example,  $T_{dB}$  can be set to 20 dB. The elements of the ML estimate of channel impulse response,  $\hat{h}_{ML}(n)$ , are selected if their energy,  $|\hat{h}_{ML}(n)|^2$ , in dB scale is larger than the value of  $\max\left\{|\hat{h}_{ML}(n)|^2\right\}_{dB} - 20dB$  (or equivalently, in linear scale, we have  $|\hat{h}_{ML}(n)|^2 \geq \max\{|\hat{h}_{ML}(n)|^2\}/T_L$ ). On the other hand, the elements whose energy (in dB scale) is smaller than the value of  $\max\left\{|\hat{h}_{ML}(n)|^2\right\}_{dB} - 20dB$  are discarded and set as zero.

Finally, the refined estimate after the threshold setting path selection method,  $\hat{\mathbf{h}}_{th}$ , is transformed back to frequency domain to get the estimated channel frequency response, i.e.,

$$\hat{\mathbf{H}}_{th} = FFT\{\hat{\mathbf{h}}_{th}\}. \quad (4.3)$$



## 4.2 Number of Path Setting Method

To improve the ML estimate of channel impulse response, the number of path setting method first defines a parameter  $N_p$ , which represents the desired number of paths. Only  $N_p$  elements with larger amplitudes in  $\hat{\mathbf{h}}_{ML}$  are preserved and the other paths are discarded. In consequence, the algorithm of the number of path setting method is presented in the following: [7]

$$\hat{h}_p(n) = \begin{cases} \hat{h}_{ML}(n), & \text{if } |\hat{h}_{ML}(n)| \text{ is one of the } N_p \text{ larger values} \\ 0, & \text{otherwise} \end{cases} \quad (4.4)$$

for  $n = 0, \dots, G-1$ .

For example, let  $N_p$  be 10. Then, only 10 elements with larger amplitude are said to be the valid elements while the remaining paths are considered as noise and set as zero.

Similar to the threshold setting method, the refined estimate,  $\hat{\mathbf{h}}_p$ , is finally transformed back to frequency domain to get the estimated channel frequency response, that is,

$$\hat{\mathbf{H}}_p = FFT\{\hat{\mathbf{h}}_p\}. \quad (4.5)$$



# Chapter 5

## Proposed Path Selection Method

Although the conventional path selection methods in the previous chapter, including the threshold setting method and the number of path setting method, are widely used for improving channel estimation, the drawback of these two methods is that they are heuristic approach to the problem and sensitive to channel power delay profiles as well as the operating SNR.

In general, how to set the threshold,  $T_{dB}$ , in the threshold setting method, is relevant to the structure of multipath power delay profiles. If the threshold is set too large, the path selection method might pick noise. On the other hand, if the threshold is set too small, the path selection method might lose true channel paths. Therefore, it is difficult to set a proper threshold for all kinds of channel environments, and improper setting of the threshold will decrease the performance of channel estimation significantly.

As to the number of path setting method, it is also difficult to know how many paths exist in wireless channel environments. Thus, it is potentially required to estimate channel length to choose a proper parameter  $N_p$  that represents the desired number of paths, or the system may suffer from performance degradation. Similar to the threshold setting method,

$N_p$  with a too large value makes noise included in the estimated channel impulse response, and  $N_p$  with a too small value excludes the true channel paths in the estimated channel impulse response.

As shown in Figure 6.45 and 6.46 in the next chapter, the simulation results show that inaccurate path selection raises the average SE of channel estimation, especially for the case of losing channel paths. Furthermore, inaccurate path selection influences not only the BER performance of the system, but also the complexity of channel tracking since the channel paths are usually tracked path-by-path in the tracking stage. Selecting more paths than the true channel paths existing in practical environments increases the complexity of the channel tracking. For example, in a two-path channel, the complexity of picking 10 paths in path selection methods is fivefold than the complexity of picking 2 paths.

According to the aforementioned discussion, we find that the conventional path selection methods are sensitive to the setting of parameters, channel conditions and the operating SNR. Thus, we would like to develop a novel path selection method which can improve the BER performance, reduce the average SE of channel estimation, and increase the probability of picking correct paths. The cost function for the proposed path selection method is then presented in the next section.

## 5.1 Cost Function

Eq.(5.1) and Eq.(5.2) represent the ML estimate for channel impulse response by using the signals on even and odd subcarriers, respectively:

$$\hat{\mathbf{h}}_{\text{even}} = \frac{2}{\sigma_x^2} \mathbf{F}_{\text{even}}^H \mathbf{X}_{\text{even}}^H \mathbf{Y}_{\text{even}} / \sqrt{N} \quad (5.1)$$

and

$$\hat{\mathbf{h}}_{\text{odd}} = \frac{2}{\sigma_x^2} \mathbf{F}_{\text{odd}}^H \mathbf{X}_{\text{odd}}^H \mathbf{Y}_{\text{odd}} / \sqrt{N}. \quad (5.2)$$

where  $\hat{\mathbf{h}}_{\text{even}}$  and  $\hat{\mathbf{h}}_{\text{odd}}$  are both of size  $(G, 1)$ ,  $\mathbf{F}_{\text{even}}$  and  $\mathbf{F}_{\text{odd}}$  are the truncated FFT matrices of size  $(N/2, G)$ ,  $\mathbf{Y}_{\text{even}}$  and  $\mathbf{Y}_{\text{odd}}$  are the received signal vectors of size  $(N/2, 1)$ ,  $\mathbf{X}_{\text{even}}$  and  $\mathbf{X}_{\text{odd}}$  are the diagonal matrices of size  $(N/2, N/2)$  and their diagonal elements are the transmitted pilot signals  $X(k)$ , and  $\sigma_x^2$  is the energy of the transmitted pilot signal, i.e.,  $\sigma_x^2 = |X(k)|^2$ . The subindices “even” and “odd” indicate vectors (or matrices) which involve even and odd subcarriers, respectively.

Afterward, a variable  $\mathbf{A}$  which is a diagonal matrix of size  $(G, G)$  is further introduced to indicate which elements in  $\hat{\mathbf{h}}_{\text{even}}$  and  $\hat{\mathbf{h}}_{\text{odd}}$  are desired paths. Thus, the cost function for the proposed path selection method can be formulated as follows:

$$\min_{\mathbf{A}} \left\| \hat{\mathbf{h}}_{\text{even}} - \mathbf{A} \hat{\mathbf{h}}_{\text{odd}} \right\|^2 + \left\| \hat{\mathbf{h}}_{\text{odd}} - \mathbf{A} \hat{\mathbf{h}}_{\text{even}} \right\|^2, \quad (5.3)$$

where the diagonal elements of  $\mathbf{A}$  are  $\{A(0), \dots, A(G-1)\}$ , each of which is either 0 or 1.

We would like to find  $\mathbf{A}$  that minimizes the SE of Eq.(5.3). The estimate of  $A(n)$  is

denoted as  $\hat{A}(n)$ . If  $\hat{A}(n)=1$ , the  $n$ th element of  $\hat{\mathbf{h}}$  is considered as a valid path; otherwise, we treat the element as noise and let  $\hat{h}(n)=0$ , where  $\hat{\mathbf{h}} = (\hat{\mathbf{h}}_{\text{odd}} + \hat{\mathbf{h}}_{\text{even}}) / 2 = [\hat{h}(0), \dots, \hat{h}(G-1)]^T$ .

To examine the meaning of our cost function, we have the following equations by substituting Eq.(3.3) into Eq.(5.2):

$$\begin{aligned}
\hat{\mathbf{h}}_{\text{odd}} &= \frac{2}{\sigma_x^2} \mathbf{F}_{\text{odd}}^H \mathbf{X}_{\text{odd}}^H (\sqrt{N} \mathbf{X}_{\text{odd}} \mathbf{H}_{\text{odd}} + \mathbf{Z}_{\text{odd}}) / \sqrt{N} \\
&= \frac{2}{\sigma_x^2} \mathbf{F}_{\text{odd}}^H \mathbf{X}_{\text{odd}}^H (\mathbf{X}_{\text{odd}} \mathbf{F}_{\text{odd}} \mathbf{h} + \mathbf{Z}_{\text{odd}} / \sqrt{N}) \\
&= \frac{2}{\sigma_x^2} (\mathbf{F}_{\text{odd}}^H \mathbf{X}_{\text{odd}}^H \mathbf{X}_{\text{odd}} \mathbf{F}_{\text{odd}} \mathbf{h} + \mathbf{F}_{\text{odd}}^H \mathbf{X}_{\text{odd}}^H \mathbf{Z}_{\text{odd}} / \sqrt{N}) \\
&= \frac{2}{\sigma_x^2} (\sigma_x^2 \frac{1}{2} \mathbf{h} + \mathbf{F}_{\text{odd}}^H \mathbf{X}_{\text{odd}}^H \mathbf{Z}_{\text{odd}} / \sqrt{N}) \\
&= \mathbf{h} + \tilde{\mathbf{z}}_1,
\end{aligned} \tag{5.4}$$

where  $\tilde{\mathbf{z}}_1 = (2 / \sigma_x^2) \mathbf{F}_{\text{odd}}^H \mathbf{X}_{\text{odd}}^H \mathbf{Z}_{\text{odd}} / \sqrt{N}$ . Similarly, we have

$$\hat{\mathbf{h}}_{\text{even}} = \mathbf{h} + \tilde{\mathbf{z}}_2, \tag{5.5}$$

where  $\tilde{\mathbf{z}}_2 = (2 / \sigma_x^2) \mathbf{F}_{\text{even}}^H \mathbf{X}_{\text{even}}^H \mathbf{Z}_{\text{even}} / \sqrt{N}$ . Eq.(5.4) and Eq.(5.5) show that  $\hat{\mathbf{h}}_{\text{odd}}$  and  $\hat{\mathbf{h}}_{\text{even}}$  could be deemed as the estimated channel impulse response (corresponding to channel  $\mathbf{h}$ ), corrupted by noise. Note that the elements of  $\tilde{\mathbf{z}}_1$  and  $\tilde{\mathbf{z}}_2$  are denoted as  $\tilde{z}_1(n)$  and  $\tilde{z}_2(n)$ , respectively, for  $n=0,1,\dots,G-1$ , each of which is with zero-mean and variance  $2\sigma_n^2 / (\sigma_x^2 N)$ .



The meaning of the cost function can be analyzed by substituting Eq.(5.4) and Eq.(5.5) into Eq.(5.3). We discuss the problem with two cases: a path does or does not exist at the  $n$ th element. When there is indeed a path at the  $n$ th element of  $\mathbf{h}$ , if  $A(n) = 1$ , the cost function with respect to the  $n$ th element of Eq(5.3) becomes as

$$|\tilde{z}_1(n) - \tilde{z}_2(n)|^2 + |\tilde{z}_2(n) - \tilde{z}_1(n)|^2 \quad (5.6)$$

and if  $A(n) = 0$ , the cost function with respect to the  $n$ th element of Eq(5.3) becomes as

$$|h(n) + \tilde{z}_1(n)|^2 + |h(n) + \tilde{z}_2(n)|^2. \quad (5.7)$$

As we can see, value of Eq(5.7) tends to be larger than value of Eq(5.6) when the amplitude of a channel path is sufficiently larger than noise, and this result sides with the solution of  $A(n) = 1$ . On the other hand, when there is no path at the  $n$ th element of  $\mathbf{h}$ , if  $A(n) = 1$ , the cost function with respect to the  $n$ th element of Eq(5.3) becomes as

$$|\tilde{z}_1(n) - \tilde{z}_2(n)|^2 + |\tilde{z}_2(n) - \tilde{z}_1(n)|^2 \quad (5.8)$$

and if  $A(n) = 0$ , the cost function with respect to the  $n$ th element of Eq(5.3) becomes as

$$|\tilde{z}_1(n)|^2 + |\tilde{z}_2(n)|^2. \quad (5.9)$$

In this case, the variance of Eq(5.8) is twice the variance of Eq(5.9), and this result sides with the solution of  $A(n) = 0$ .

## 5.2 Optimum Solution

To solve the minimization problem in Eq(5.3), we expand it as follows:

$$\begin{aligned}
& \min_{\mathbf{A}} \left\| \hat{\mathbf{h}}_{\text{even}} - \mathbf{A}\hat{\mathbf{h}}_{\text{odd}} \right\|^2 + \left\| \hat{\mathbf{h}}_{\text{odd}} - \mathbf{A}\hat{\mathbf{h}}_{\text{even}} \right\|^2 \\
&= \min_{\mathbf{A}} \left( \hat{\mathbf{h}}_{\text{even}} - \mathbf{A}\hat{\mathbf{h}}_{\text{odd}} \right)^H \left( \hat{\mathbf{h}}_{\text{even}} - \mathbf{A}\hat{\mathbf{h}}_{\text{odd}} \right) + \left( \hat{\mathbf{h}}_{\text{odd}} - \mathbf{A}\hat{\mathbf{h}}_{\text{even}} \right)^H \left( \hat{\mathbf{h}}_{\text{odd}} - \mathbf{A}\hat{\mathbf{h}}_{\text{even}} \right) \\
&= \min_{\mathbf{A}} \hat{\mathbf{h}}_{\text{even}}^H \hat{\mathbf{h}}_{\text{even}} - \hat{\mathbf{h}}_{\text{even}}^H \mathbf{A}\hat{\mathbf{h}}_{\text{odd}} - \hat{\mathbf{h}}_{\text{odd}}^H \mathbf{A}\hat{\mathbf{h}}_{\text{even}} + \hat{\mathbf{h}}_{\text{odd}}^H \mathbf{A}\hat{\mathbf{h}}_{\text{odd}} \\
&\quad + \hat{\mathbf{h}}_{\text{odd}}^H \hat{\mathbf{h}}_{\text{odd}} - \hat{\mathbf{h}}_{\text{odd}}^H \mathbf{A}\hat{\mathbf{h}}_{\text{even}} - \hat{\mathbf{h}}_{\text{even}}^H \mathbf{A}\hat{\mathbf{h}}_{\text{odd}} + \hat{\mathbf{h}}_{\text{even}}^H \mathbf{A}\hat{\mathbf{h}}_{\text{even}} \\
&= \min_{\mathbf{A}} \text{tr} \left( -\hat{\mathbf{h}}_{\text{even}}^H \mathbf{A}\hat{\mathbf{h}}_{\text{odd}} - \hat{\mathbf{h}}_{\text{odd}}^H \mathbf{A}\hat{\mathbf{h}}_{\text{even}} + \hat{\mathbf{h}}_{\text{odd}}^H \mathbf{A}\hat{\mathbf{h}}_{\text{odd}} \right. \\
&\quad \left. - \hat{\mathbf{h}}_{\text{odd}}^H \mathbf{A}\hat{\mathbf{h}}_{\text{even}} - \hat{\mathbf{h}}_{\text{even}}^H \mathbf{A}\hat{\mathbf{h}}_{\text{odd}} + \hat{\mathbf{h}}_{\text{even}}^H \mathbf{A}\hat{\mathbf{h}}_{\text{even}} \right) \\
&= \min_{\mathbf{A}} \text{tr} \left( -\hat{\mathbf{h}}_{\text{odd}} \hat{\mathbf{h}}_{\text{even}}^H \mathbf{A} - \hat{\mathbf{h}}_{\text{even}} \hat{\mathbf{h}}_{\text{odd}}^H \mathbf{A} + \hat{\mathbf{h}}_{\text{odd}} \hat{\mathbf{h}}_{\text{odd}}^H \mathbf{A} \right. \\
&\quad \left. - \hat{\mathbf{h}}_{\text{even}} \hat{\mathbf{h}}_{\text{odd}}^H \mathbf{A} - \hat{\mathbf{h}}_{\text{odd}} \hat{\mathbf{h}}_{\text{even}}^H \mathbf{A} + \hat{\mathbf{h}}_{\text{even}} \hat{\mathbf{h}}_{\text{even}}^H \mathbf{A} \right) \\
&= \min_{\mathbf{A}} \text{tr} \left( \left( \hat{\mathbf{h}}_{\text{odd}} \hat{\mathbf{h}}_{\text{odd}}^H + \hat{\mathbf{h}}_{\text{even}} \hat{\mathbf{h}}_{\text{even}}^H - 4\Re \left( \hat{\mathbf{h}}_{\text{odd}} \hat{\mathbf{h}}_{\text{even}}^H \right) \right) \mathbf{A} \right)
\end{aligned} \tag{5.10}$$

Let us define a matrix  $\mathbf{f}$  as follows:

$$\mathbf{f} = \left( \hat{\mathbf{h}}_{\text{odd}} \hat{\mathbf{h}}_{\text{odd}}^H + \hat{\mathbf{h}}_{\text{even}} \hat{\mathbf{h}}_{\text{even}}^H \right) - 4\Re \left( \hat{\mathbf{h}}_{\text{odd}} \hat{\mathbf{h}}_{\text{even}}^H \right). \tag{5.11}$$

Obviously, the minimization problem of Eq.(5.10) can be viewed as an ILP problem or a 0-1 programming problem; that is, we have [10]:

$$\min_{\mathbf{A}} \{ f(0)A(0) + f(1)A(1) + \dots + f(L-1)A(L-1) \}, \tag{5.12}$$

where  $A(n)$  and  $f(n)$ , for  $n=0, \dots, G-1$ , are diagonal elements of  $\mathbf{A}$  and  $\mathbf{f}$ , respectively.

Since the optimum solution of a linear programming (LP) problem can only be vertices

of the feasible set [10], the ILP problem of Eq.(5.14) can be equivalently transformed into a simple LP problem. To do this, we use  $0 \leq A(n) \leq 1$ , for  $n = 0, \dots, G-1$  instead of the integer constraint of  $A(n)$ , i.e.,  $A(n) = 0$  or  $1$ . The process of this constraint release is reasonable because for this new constraint, each element of the vertices in the feasible set is either 0 or 1. Consequently, the ILP problem of Eq(5.12) can be transformed into a simple LP. Even though the LP problem can be solved by the simplex method, the computation still requires considerable effort to achieve the optimal solution. In order to reduce the computation complexity, we then develop a more simple method to find the optimum solution. In fact, it can be easily observed that the optimum solution of Eq(5.12) is to make  $A(n)$  corresponding to the negative value of  $f(n)$  be one; otherwise,  $A(n)$  is set to zero. As a result, we have the optimum solution of Eq(5.14):

$$\hat{A}(n) = \begin{cases} 1, & \text{if } f(n) < 0 \\ 0, & \text{otherwise} \end{cases} \quad (5.13)$$

for  $n = 0, \dots, G-1$ .

### 5.3 Refined Path Selection Method

In the following subsections, we further propose a refined path selection method to suppress noise and reduce the probability of false alarm by finding a proper threshold which is insensitive to channel power delay profiles.

### 5.3.1 Analysis of False Alarm

By substituting Eq.(5.4) and Eq.(5.5) into Eq.(5.11), we can obtain

$$\begin{aligned}
\mathbf{f} &= (\hat{\mathbf{h}}_{\text{odd}} \hat{\mathbf{h}}_{\text{odd}}^H + \hat{\mathbf{h}}_{\text{even}} \hat{\mathbf{h}}_{\text{even}}^H) - 4\Re e(\hat{\mathbf{h}}_{\text{odd}} \hat{\mathbf{h}}_{\text{even}}^H) \\
&= (\mathbf{h} + \tilde{\mathbf{z}}_1)(\mathbf{h} + \tilde{\mathbf{z}}_1)^H + (\mathbf{h} + \tilde{\mathbf{z}}_2)(\mathbf{h} + \tilde{\mathbf{z}}_2)^H - 4\Re e((\mathbf{h} + \tilde{\mathbf{z}}_1)(\mathbf{h} + \tilde{\mathbf{z}}_2)^H) \\
&= \mathbf{h}\mathbf{h}^H + \tilde{\mathbf{z}}_1 \tilde{\mathbf{z}}_1^H + \tilde{\mathbf{z}}_1 \mathbf{h}^H + \mathbf{h} \tilde{\mathbf{z}}_1^H + \mathbf{h}\mathbf{h}^H + \tilde{\mathbf{z}}_2 \tilde{\mathbf{z}}_2^H + \tilde{\mathbf{z}}_2 \mathbf{h}^H + \mathbf{h} \tilde{\mathbf{z}}_2^H \\
&\quad - 4\Re e(\mathbf{h}\mathbf{h}^H + \tilde{\mathbf{z}}_1 \tilde{\mathbf{z}}_2^H + \mathbf{h} \tilde{\mathbf{z}}_2^H + \tilde{\mathbf{z}}_1 \mathbf{h}^H) \\
&= 2\mathbf{h}\mathbf{h}^H + \tilde{\mathbf{z}}_1 \tilde{\mathbf{z}}_1^H + \tilde{\mathbf{z}}_2 \tilde{\mathbf{z}}_2^H - 4\Re e(\mathbf{h}\mathbf{h}^H) - 2\Re e(\tilde{\mathbf{z}}_1 \mathbf{h}^H) - 2\Re e(\tilde{\mathbf{z}}_2 \mathbf{h}^H) - 4\Re e(\tilde{\mathbf{z}}_1 \tilde{\mathbf{z}}_2^H)
\end{aligned} \tag{5.14}$$

According to Eq.(5.13), the analysis of false alarm can be done point-by-point due to the fact that the value of  $\hat{A}(n)$  merely depends on the value of  $f(n)$  and the elements of  $\tilde{\mathbf{z}}_1$  and  $\tilde{\mathbf{z}}_2$  are i.i.d. Assuming that  $h(n) = 0$ , we can therefore calculate  $f(n)$  as

$$f(n) = \tilde{z}_1(n) \tilde{z}_1^H(n) + \tilde{z}_2(n) \tilde{z}_2^H(n) - 4\Re e(\tilde{z}_1(n) \tilde{z}_2^H(n)), \tag{5.15}$$

It is noted that when the value of  $f(n)$  in Eq.(5.15) is negative, false alarm occurs at the position  $n$ . Instead of deriving a closed-form probability density function (PDF) for the variable  $f(n)$  in Eq.(5.15), we use bootstrap (or resampling) techniques in Monte Carlo methods to simulate the PDF. The basic idea of the bootstrap is to evaluate the PDF through the empirical samples [11], and the PDF of  $f(n)$  in Eq.(5.15) is then simulated in Figure 5.1. As shown in Figure 5.1, even if there is no path at the position  $n$ , there is still a certain probability for the negative value of  $f(n)$ , resulting in the event of false alarm. Although the range of the values for the variable  $f(n)$  in Eq.(5.15) varies with the variance of  $Z(k)$ , the shape and proportion of the PDF is invariant to the value of

$\sigma_n^2 / (\sigma_x^2 N)$ . To reduce the probability of false alarm, we propose a refined path selection method in the next subsection.

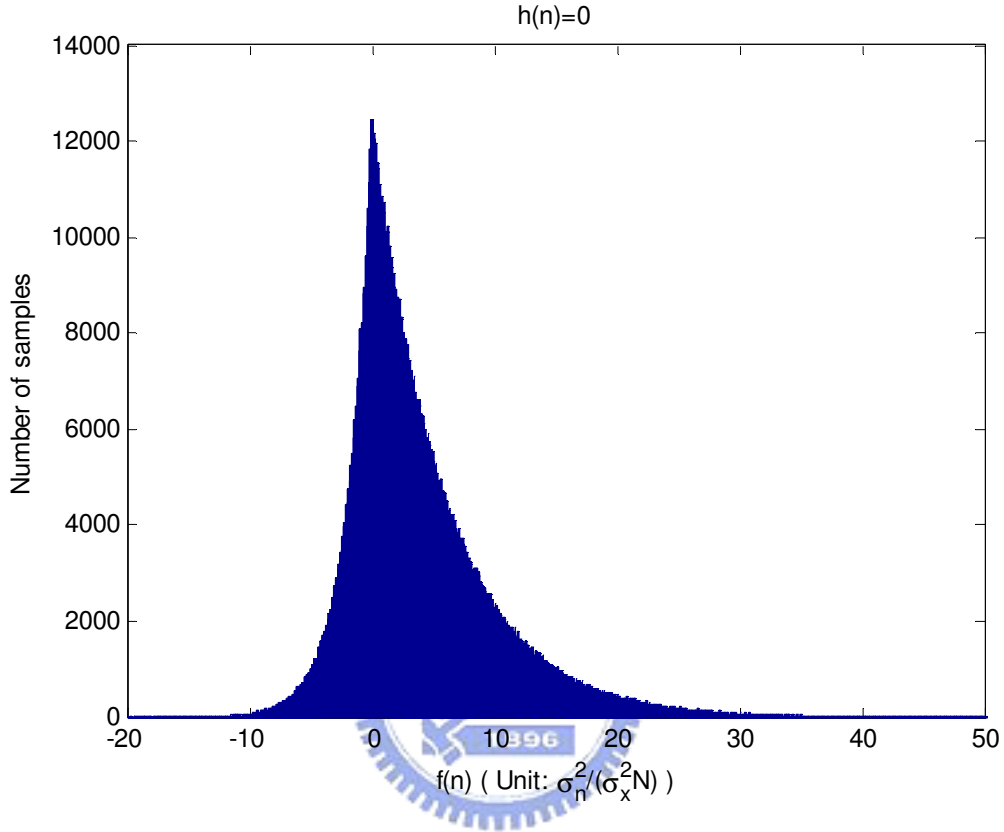


Figure 5.1 The PDF of  $f(n)$  evaluated through the empirical samples with 1,000,000 samples.

### 5.3.2 Algorithm

Since the channel length is less than  $G$ , the values of  $f(n)$ , for those positions  $n = G, \dots, (N/2) - 1$  corresponding to  $h(n) = 0$ , can be looked upon as samples which are generated from the random variable  $f(n)$ . Therefore, we propose the refined path selection method to suppress noise and to reduce the probability of false alarm in the following:

$$\hat{A}(n) = \begin{cases} 1, & \text{if } f(n) < R_{th} \\ 0, & \text{otherwise} \end{cases} \quad (5.16)$$

for  $n=0,1,\dots,G-1$  and  $R_{th} = -U \times \max\{f(n)\}$ , for  $n=G,\dots,(N/2)-1$ , where the value of  $U$  is to be determined.

### 5.3.3 Determination of the Parameter $U$

The determination of the value of the parameter  $U$  will depend on the probability of false alarm and miss detection. Moreover, the probability of miss detection is related to the strength of a channel path. In this subsection, we first analyze the influence of the miss detection of a path on the signal-to-noise and estimation error power ratio (SNER), and develop a rule of thumb to suggest the strength of a path whose probability of miss detection should be concerned. We then develop a method to determine the value of the parameter  $U$  which can achieve a desired probability of false alarm and miss detection. Recall that  $\hat{\mathbf{h}} = (\hat{\mathbf{h}}_{\text{odd}} + \hat{\mathbf{h}}_{\text{even}})/2$ ,  $\hat{\mathbf{h}}_{\text{odd}} = \mathbf{h} + \tilde{\mathbf{z}}_2$  in Eq.(5.4), and  $\hat{\mathbf{h}}_{\text{even}} = \mathbf{h} + \tilde{\mathbf{z}}_1$  in Eq. (5.5). Note that each element of  $\hat{\mathbf{h}}$  is denoted as  $\hat{h}(n)$ . Hence, we have

$$\hat{\mathbf{h}} = \mathbf{h} + \tilde{\mathbf{z}} \quad (5.17)$$

where  $\tilde{\mathbf{z}} = (\tilde{\mathbf{z}}_1 + \tilde{\mathbf{z}}_2)/2$ , and each element of  $\tilde{\mathbf{z}}$  is denoted as  $\tilde{z}(n)$  with zero mean and variance  $\sigma_n^2 / (\sigma_x^2 N)$ . Assume that there is a channel path at position  $\bar{n}$  with path energy  $|h(\bar{n})|^2 = \mu \sigma_n^2 / (\sigma_x^2 N)$ , for  $\mu \geq 0$ . If the path  $h(\bar{n})$  is not detected, the miss detection of

this path will introduce channel estimation error  $\Delta H(k)$  in the estimated channel frequency response, i.e., we have the estimated channel frequency response:

$$\hat{H}(k) = H(k) + \Delta H(k) \quad (5.18)$$

where  $\Delta H(k) = \frac{1}{\sqrt{N}} \sum_{n=0}^{N-1} h(\bar{n}) \delta(n-\bar{n}) e^{-j2\pi kn}$ . Thus, we have

$$|\Delta H(k)|^2 = \frac{1}{N} \times \mu \frac{\sigma_n^2}{\sigma_x^2 N} \quad (5.19)$$

for  $k = 0, \dots, N-1$ . From Eq.(3.2) and Eq.(5.18), the received signal after channel matching can be written as

$$\begin{aligned} \frac{\hat{H}^*(k)}{|\hat{H}(k)|^2} Y(k) &= \frac{(H(k) + \Delta H(k))^*}{|H(k) + \Delta H(k)|^2} (\sqrt{N} X(k) H(k) + Z(k)) \\ &= \frac{(H(k) + \Delta H(k))^*}{|H(k) + \Delta H(k)|^2} (\sqrt{N} X(k) (H(k) + \Delta H(k)) + Z(k)) - \frac{(H(k) + \Delta H(k))^*}{|H(k) + \Delta H(k)|^2} \sqrt{N} X(k) \Delta H(k) \\ &= \sqrt{N} X(k) + \frac{(H(k) + \Delta H(k))^*}{|H(k) + \Delta H(k)|^2} Z(k) - \frac{(H(k) + \Delta H(k))^*}{|H(k) + \Delta H(k)|^2} \sqrt{N} X(k) \Delta H(k) \end{aligned} \quad (5.20)$$

Hence, the SNER can be calculated as

$$\begin{aligned} SNER &= \frac{N\sigma_x^2}{\frac{|H(k) + \Delta H(k)|^2}{|H(k) + \Delta H(k)|^4} \sigma_n^2 + \frac{|H(k) + \Delta H(k)|^2}{|H(k) + \Delta H(k)|^4} N\sigma_x^2 |\Delta H(k)|^2} \\ &= \frac{N\sigma_x^2 |H(k) + \Delta H(k)|^2}{\sigma_n^2 + N\sigma_x^2 |\Delta H(k)|^2} \end{aligned}$$

$$= \frac{N\sigma_x^2 |H(k) + \Delta H(k)|^2}{\sigma_n^2 + N\sigma_x^2 \times \frac{1}{N} \times \mu \frac{\sigma_n^2}{\sigma_x^2 N}} \quad (5.21)$$

$$= \frac{N\sigma_x^2 |H(k) + \Delta H(k)|^2}{\sigma_n^2 + \mu \frac{\sigma_n^2}{N}}$$

Moreover, for high SNR, we have  $N\sigma_x^2 |H(k)|^2 / \sigma_n^2 \gg 1$ . If  $N \geq \mu$ , we then have

$$|H(k)|^2 \gg \sigma_n^2 / (N\sigma_x^2) \geq |\Delta H(k)|^2 \quad (5.22)$$

By using the assumption of Eq.(5.22), SNER of Eq.(5.21) can be approximated as

$$SNER \approx \frac{N\sigma_x^2 |H(k)|^2}{\sigma_n^2 + \mu \frac{\sigma_n^2}{N}} \quad (5.23)$$

As we can observe in Eq.(5.23), when  $N \gg \mu$ , the miss detection of the path will not have significant influence on the SNER. That is, when  $N \gg \mu$ , we have

$$SNER \approx \frac{N\sigma_x^2 |H(k)|^2}{\sigma_n^2 + \mu \frac{\sigma_n^2}{N}} \approx \frac{N\sigma_x^2 |H(k)|^2}{\sigma_n^2} = SNR \quad (5.24)$$

In this thesis,  $N$  is set as 256. Hence, we will concern the probability of miss detection of a path with energy  $|h(\bar{n})|^2 = 25\sigma_n^2 / (\sigma_x^2 N)$  as a design reference, i.e., set  $\mu = 25$ .

Figure 5.2 shows the CDF of the false alarm ( $\mu = 0$ ) and the miss detection ( $\mu = 25$ ) of the variable  $f(n)$ . According to the solid line, we have  $\Pr(f(n) \geq 23.2\sigma_n^2) = 1/64$ . In other words, among  $f(n)$ , for  $n = G, \dots, (N/2) - 1$ , the occurrence of the event of



$\{f(n) \geq 23.2\sigma_n^2\}$  is  $((N/2) - G)/64$  on average. For example, when  $N$  and  $G$  are set as 256 and 64, respectively, we can acquire one point of  $f(n)$  whose value is larger than  $23.2\sigma_n^2$ , i.e., we have  $\max\{f(n)\} \geq 23.2\sigma_n^2$  and therefore  $R_{th} \leq -U \times 23.2\sigma_n^2$  (in average sense). Accordingly, Table 5.1 lists the probability of false alarm ( $\mu = 0$ ) and miss detection ( $\mu = 25$ ) with  $U$  as a parameter. We denote  $R_{Nth}$  and  $f_N(n)$  as normalized terms, i.e.,  $R_{Nth} = R_{th} / (\sigma_n^2 / (\sigma_x^2 N))$  and  $f_N(n) = f(n) / (\sigma_n^2 / (\sigma_x^2 N))$ . From this table, we can determine the value of  $U$  which can achieve a desired probability of false alarm and miss detection. In this thesis, we can choose the value of  $U$  as 0.5 such that the probability of false alarm is less than  $7.55 \times 10^{-4}$  and the probability of miss detection is larger than  $10^{-2}$ .



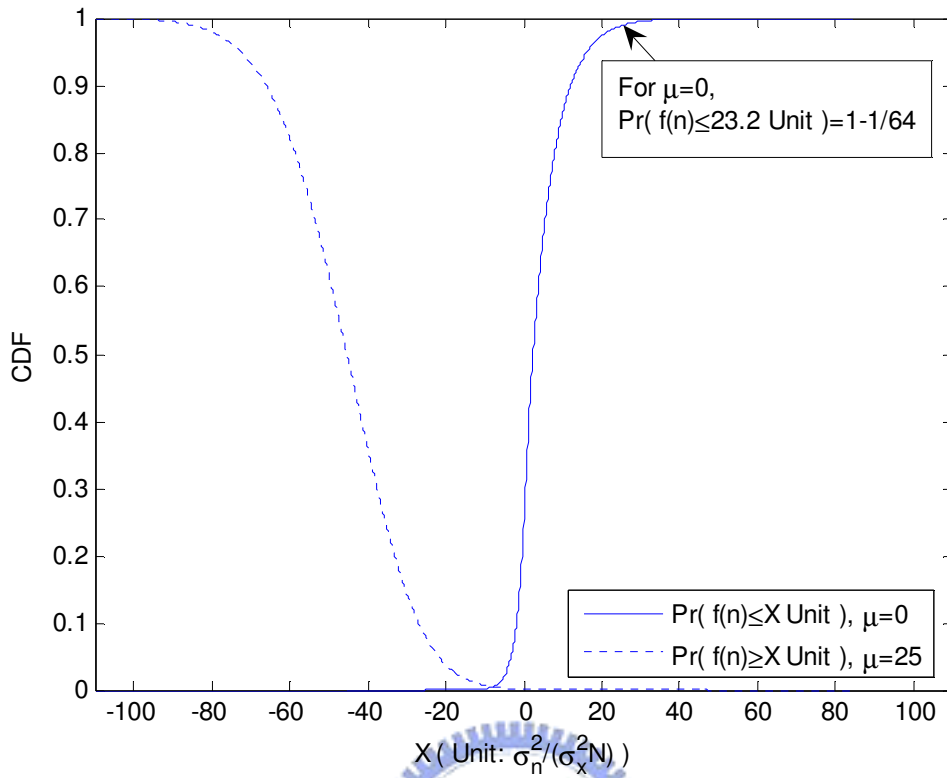


Figure 5.2 The CDF of  $f(n)$  evaluated through the empirical samples with 1,000,000 samples.

Table 5.1 The probability of false alarm and miss detection with  $U$  as a parameter.

$U$	$R_{Nth} \leq$	False Alarm ( $\mu = 0$ ): $\Pr(f_N(n) \leq R_{Nth}) \leq$	Miss Detection ( $\mu = 25$ ): $\Pr(f_N(n) \geq R_{Nth}) \geq$
0	0	0.2510	0.0014
0.1	-2.32	0.0785	0.0020
0.2	-4.64	0.0245	0.0031
0.3	-6.96	0.0076	0.0046
0.4	-9.28	0.0023	0.0067
0.5	-11.60	7.5500e-004	0.0100
0.6	-13.92	2.4400e-004	0.0146
0.7	-16.24	7.8000e-005	0.0213
0.8	-18.56	2.5000e-005	0.0307
0.9	-20.88	8.0000e-006	0.0435
1.0	-23.20	4.0000e-006	0.0610

The algorithm of Eq.(5.16) can be implemented by sorting the values of  $f(n)$ , for  $n=0,1,\dots,G-1$ , in ascending order, as shown in Figure 5.3. The refined path selection method becomes that if  $f(n)$  is smaller than the threshold  $R_{th}$ , we say that there is a valid path at the  $n$ th position, and  $\hat{A}(n)$  is set as 1; otherwise,  $\hat{A}(n)$  is set as 0. Since the threshold is determined adaptively according to the value of  $\max\{f(n)\}$ , for  $n=G,\dots,(N/2)-1$ , we can expect that the refined path selection method is more robust than the two conventional path selection methods, aforementioned in the previous chapter.

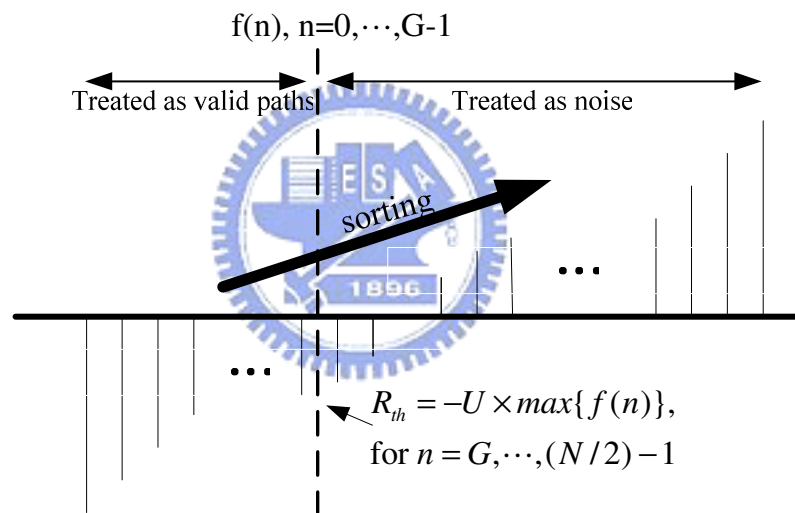


Figure 5.3 The proposed algorithm can be implemented by sorting the values of  $f(n)$ , for  $n=0,1,\dots,G-1$ , in ascending order

# Chapter 6

## Simulation Results

In this chapter, we simulate the BER, average SE and probability of picking wrong paths to demonstrate the performance of our proposed path selection method for channel estimation in OFDM systems. Besides, we also compare the performance with the two conventional path selection methods, including the number of path setting method and the threshold setting method.

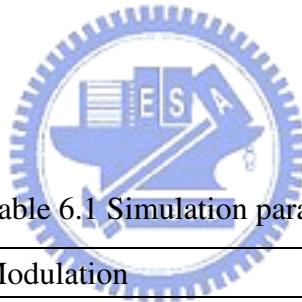


Table 6.1 Simulation parameters

Modulation	QPSK
Carrier frequency	2.3 GHZ
Total bandwidth	5 MHZ
Number of subcarriers	256
Subcarrier frequency spacing	19.53 kHz
Useful symbol time	51.2 us
Guard interval	12.8 us
Overall symbol time	64 us
Number of transmit antennas	1
Number of receive antennas	1

Table 6.2 Power delay profiles of channel environments

ITU-Veh. A channel	0, -1, -9, -10, -15, -20 (dB)
ITU-Veh. B channel	-2.5, 0, -12.8, -10, -25.2, -16 (dB)
Two-path channel	0, -1 (dB)
Thirty-path exponentially decayed channel	0, -1.3029, -2.6058, -3.9087, -5.2116, -6.5144, -7.8173, -9.1202, -10.4231, -11.7260, -13.0289, -14.3317, -15.6346, -16.9375, -18.2404, -19.5433, -20.8462, -22.1490, -23.4519, -24.7548, -26.0577, -27.3606, -28.6635, -29.9663, -31.2692, -32.5721, -33.8750, -35.1779, -36.4808, -37.7836, -39.0865 (dB)

The simulation parameters are listed in Table 6.1. Throughout the simulations, carrier frequency synchronization and symbol timing synchronization are assumed to be perfect. Moreover, the simulations are conducted at baseband using the complex low-pass equivalent representation. The ratio of energy between the pilot signal and the data signal (on a subcarrier) is set to 1.

Only the small-scale fading is considered in our simulations. Besides, we use four typical channel power delay profiles, including International Telecommunication Union (ITU)- Vehicular A and Vehicular B fading channels, a two-path equal power fading channel, and a thirty-path exponentially decayed fading channel, to demonstrate the performance. The power delay profiles defined by the recommendations of the ITU are well-established channel models for research of mobile communication systems. They specify channel conditions for various operating environments encountered in

third-generation wireless systems, e.g the Universal Mobile Telecommunication Systems (UMTS) Terrestrial Radio Access System (UTRA) standardised by 3GPP[12]. Both the Veh. A and Veh. B channels are six-path channels with power delay profiles: 0, -1, -9, -10, -15, -20 (dB) and -2.5, 0, -12.8, -10, -25.2, -16 (dB), respectively. For the two-path equal power fading channel, the power delay profile is 0, 0 (dB). For the thirty-path exponentially decayed fading channel, the power delay profile (linear scale) is given by [13]:

$$\alpha \times \exp(-\beta \times l), \text{ for } l = 0, \dots, L-1$$

where  $\alpha = \frac{1 - \exp(-\beta)}{1 - \exp(-L \times \beta)}$  is a normalization term keeping the total power of paths equal

to unity and  $\beta$  is a decaying factor and  $L = 30$ . For the value of  $\beta = 0.3$ , the power delay profile of the thirty-path channel is listed in Table 6.2.



# 6.1 Threshold for Refined Path Selection

## Method

In Section 5.3, we set the value of  $U$  as 0.5 for the threshold  $R_{th} = -U \times \max\{f(n)\}$  in the refined path selection method. The algorithm of the refined path selection method is that if  $f(n)$  is smaller than the threshold  $R_{th} = -0.5 \times \max\{f(n)\}$ , we say that there is a channel path at the  $n$ th position, and  $\hat{A}(n)$  is set as 1; otherwise,  $\hat{A}(n)$  is set as 0.

In this section, computer simulations are conducted in the ITU-Veh. A channel, the thirty-path channel, and the two-path channel to verify if the threshold  $R_{th} = -0.5 \times \max\{f(n)\}$  is appropriate and robust for practical use. The value of  $U$  is simulated from 0 to -6. Figure 6.1 and Figure 6.3 show the BER performance for the proposed path selection method in the Veh. A channel at  $E_b/N_0 = 10\text{dB}$  and  $40\text{dB}$ , respectively, with  $U$  as a parameter. Figure 6.2 and Figure 6.4 show the average SE performance for the proposed path selection method in the Veh. A channel at  $E_b/N_0 = 10\text{dB}$  and  $40\text{dB}$ , respectively, with  $U$  as a parameter. Figure 6.5 and Figure 6.7 show the BER performance for the proposed path selection method in the thirty-path channel at  $E_b/N_0 = 10\text{dB}$  and  $40\text{dB}$ , respectively, with  $U$  as a parameter. Figure 6.6 and Figure 6.8 show the average SE performance for the proposed path selection method in the thirty-path channel at  $E_b/N_0 = 10\text{dB}$  and  $40\text{dB}$ , respectively, with  $U$  as a parameter. Figure 6.9 and

Figure 6.11 show the BER performance for the proposed path selection method in the two-path channel at  $E_b/N_0=10\text{dB}$  and  $40\text{dB}$ , respectively, with  $U$  as a parameter. Figure 6.10 and Figure 6.12 show the average SE performance for the proposed path selection method in the two-path channel at  $E_b/N_0 = 10\text{dB}$  and  $40\text{dB}$ , respectively, with  $U$  as a parameter.

We can observe that for the BER performance shown in Figure 6.1, Figure 6.3, Figure 6.5, Figure 6.7, Figure 6.9, and Figure 6.11, the threshold  $R_{th}$  which ranges from  $0$  to  $-6 \times \max\{f(n)\}$  has no significant influence on BER performance of our proposed method. As shown in Fig. 6.2 and Fig. 6.4, we can find that for the Veh. A channel, the minimum average SE is achieved at a threshold between  $-0.4 \times \max\{f(n)\}$  and  $-0.6 \times \max\{f(n)\}$ . Moreover, as shown in Figure 6.6 and Figure 6.8, we can find that for the thirty-path channel, the minimum average SE is achieved at a threshold between  $-0.2 \times \max\{f(n)\}$  and  $-0.4 \times \max\{f(n)\}$ . In Figure 6.10 and Figure 6.12, we can also observe that a threshold between  $-0.6 \times \max\{f(n)\}$  and  $-0.8 \times \max\{f(n)\}$  can attain the minimum average SE in the two-path channel. As a result, we can conclude that  $R_{th} = -0.5 \times \max\{f(n)\}$  is an appropriate value for the setting of the threshold in the refined path selection method.



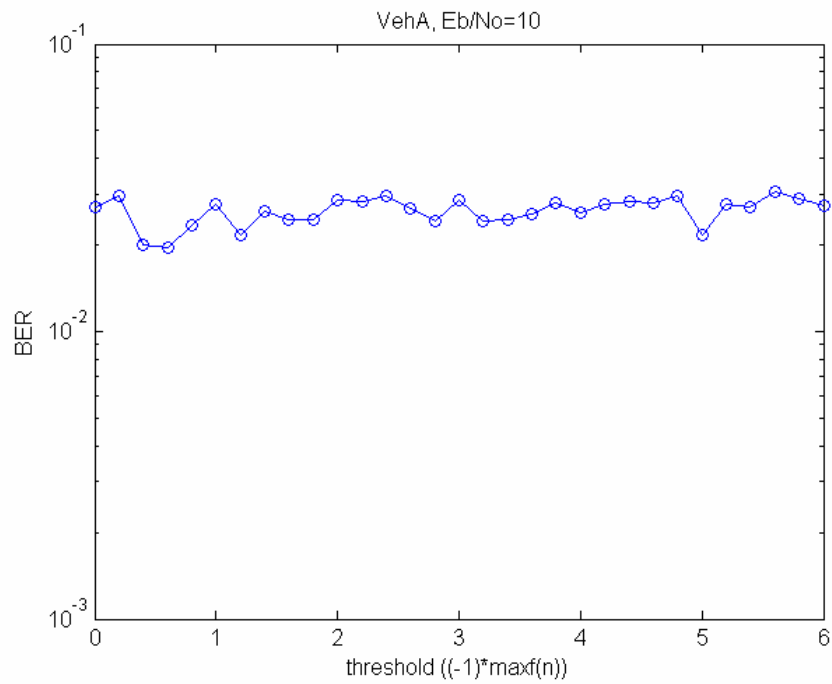


Figure 6.1 The BER performance for the proposed path selection method in the Veh. A channel at  $E_b/N_0 = 10\text{dB}$  with threshold as a parameter.

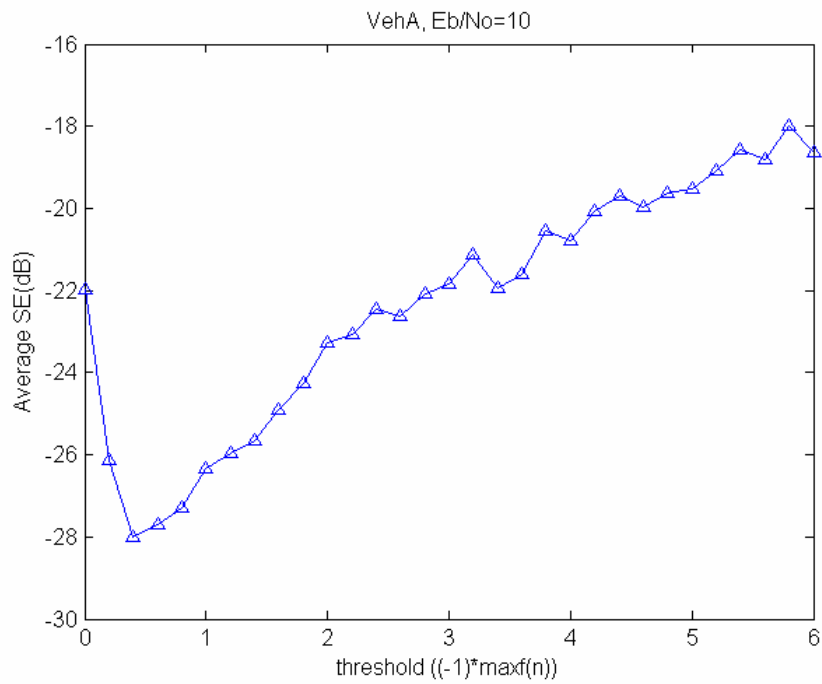


Figure 6.2 The average SE for the proposed path selection method in the Veh. A channel at  $E_b/N_0 = 10\text{dB}$  with threshold as a parameter.

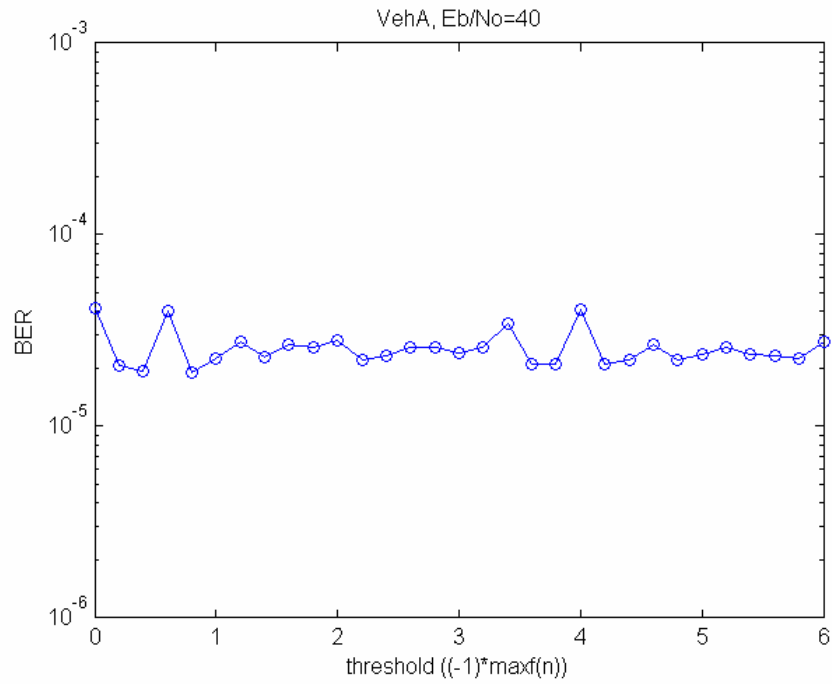


Figure 6.3 The BER performance for the proposed path selection method in the Veh. A channel at  $E_b/N_0 = 40\text{dB}$  with threshold as a parameter.

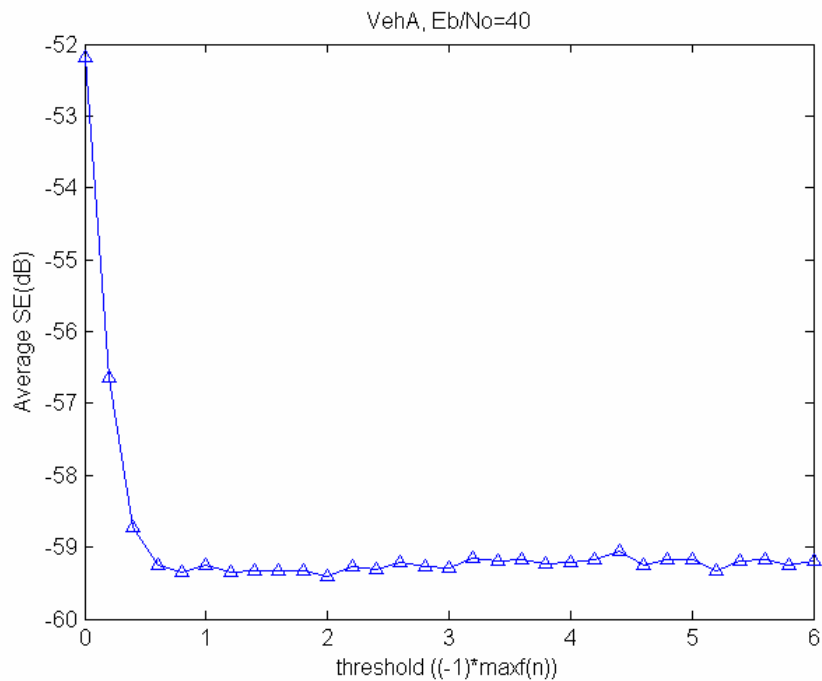


Figure 6.4 The average SE for the proposed path selection method in the Veh. A channel at  $E_b/N_0 = 40\text{dB}$  with threshold as a parameter.

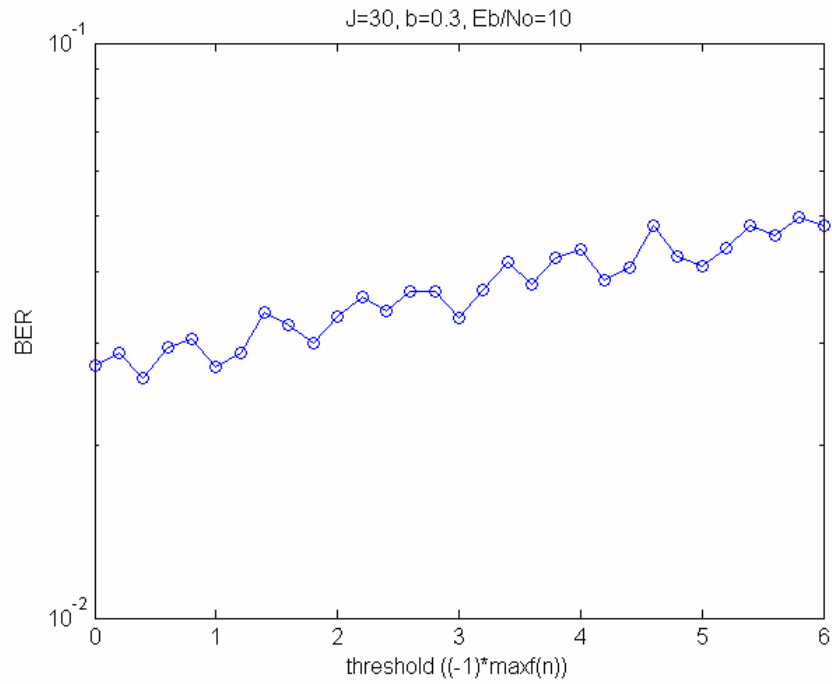


Figure 6.5 The BER performance for the proposed path selection method in the thirty-path channel at  $E_b/N_0 = 10\text{dB}$  with threshold as a parameter.

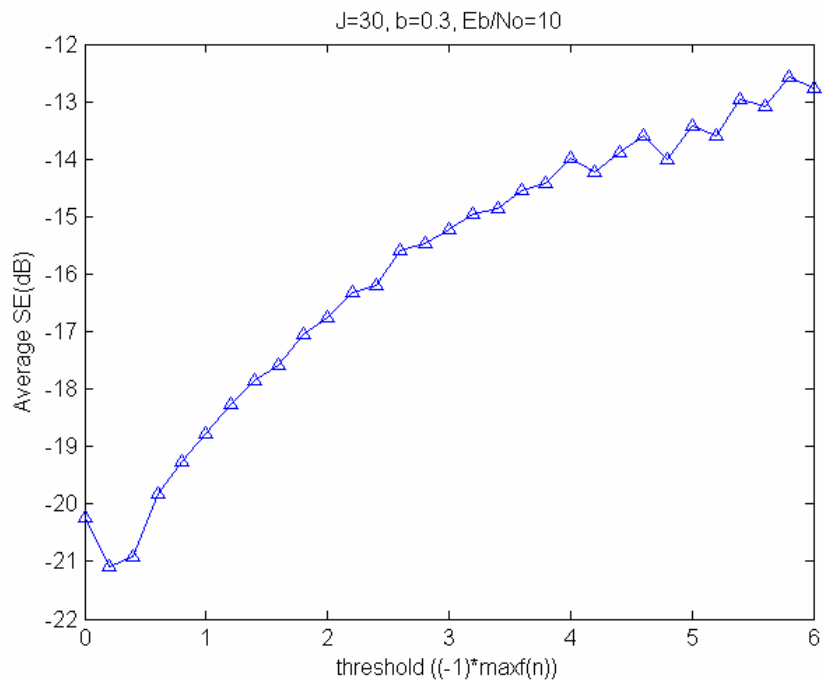


Figure 6.6 The average SE for the proposed path selection method in the thirty-path channel at  $E_b/N_0 = 10\text{dB}$  with threshold as a parameter.

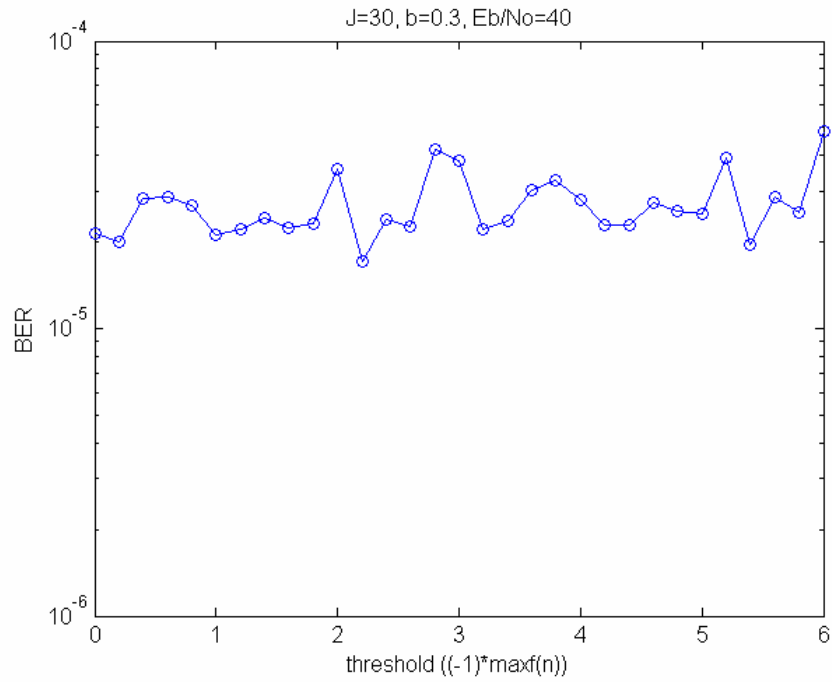


Figure 6.7 The BER performance for the proposed path selection method in the thirty-path channel at  $E_b/N_0 = 40\text{dB}$  with threshold as a parameter.

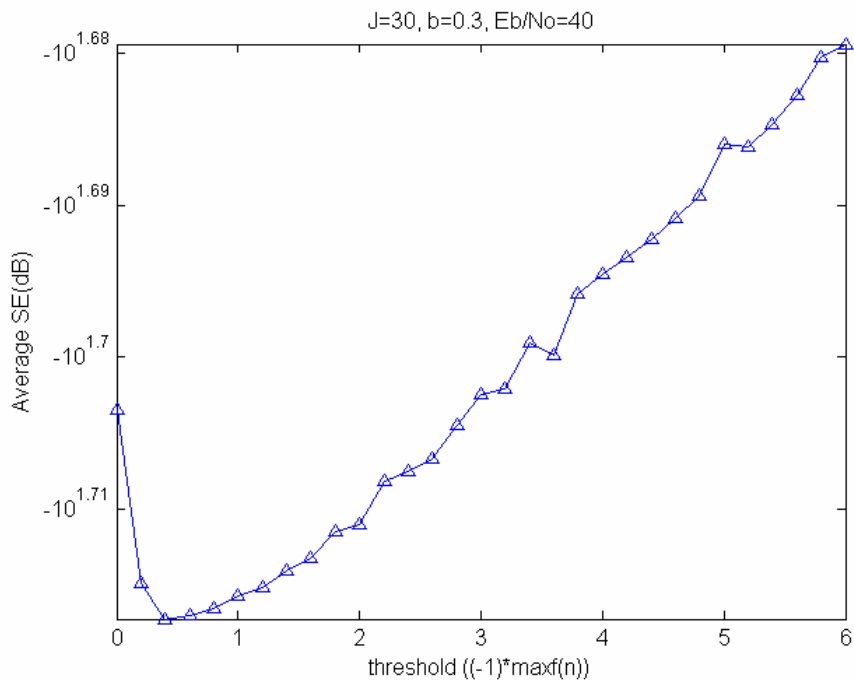


Figure 6.8 The average SE for the proposed path selection method in the thirty-path channel at  $E_b/N_0 = 40\text{dB}$  with threshold as a parameter.

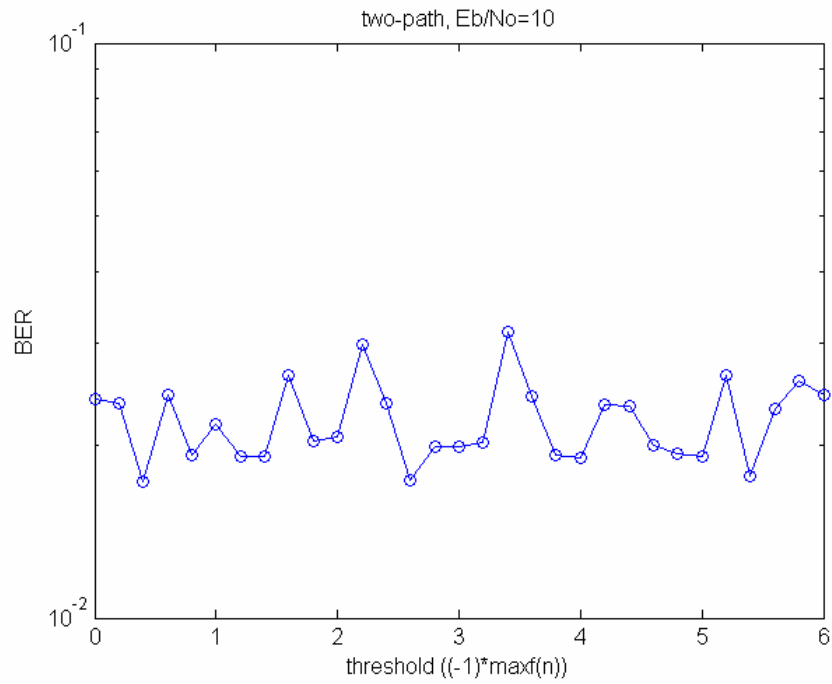


Figure 6.9 The BER performance for the proposed path selection method in the two-path channel at  $E_b/N_0 = 10\text{dB}$  with threshold as a parameter.

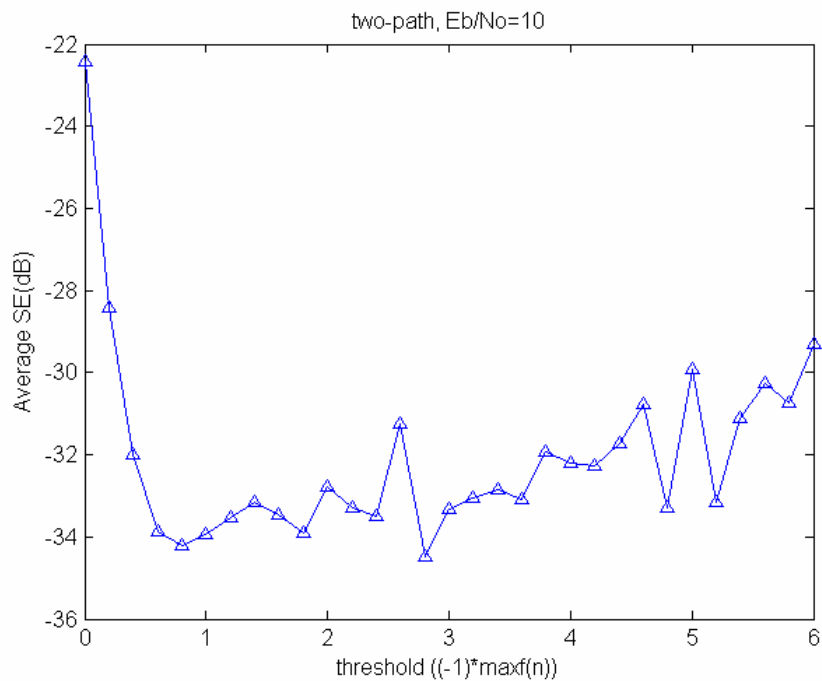


Figure 6.10 The average SE for the proposed path selection method in the two-path channel at  $E_b/N_0 = 10\text{dB}$  with threshold as a parameter.

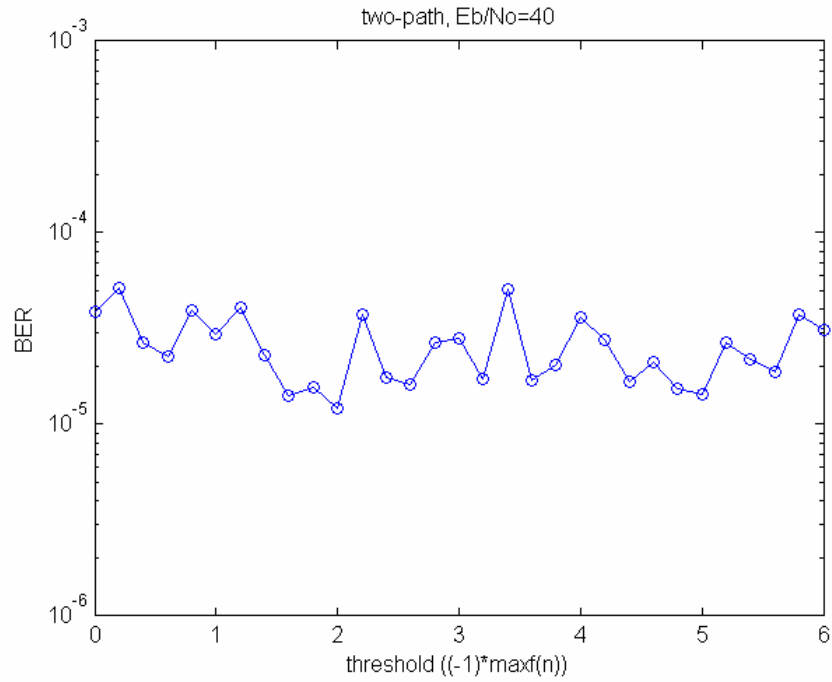


Figure 6.11 The BER performance for the proposed path selection method in the two-path channel at  $E_b/N_0 = 40\text{dB}$  with threshold as a parameter.

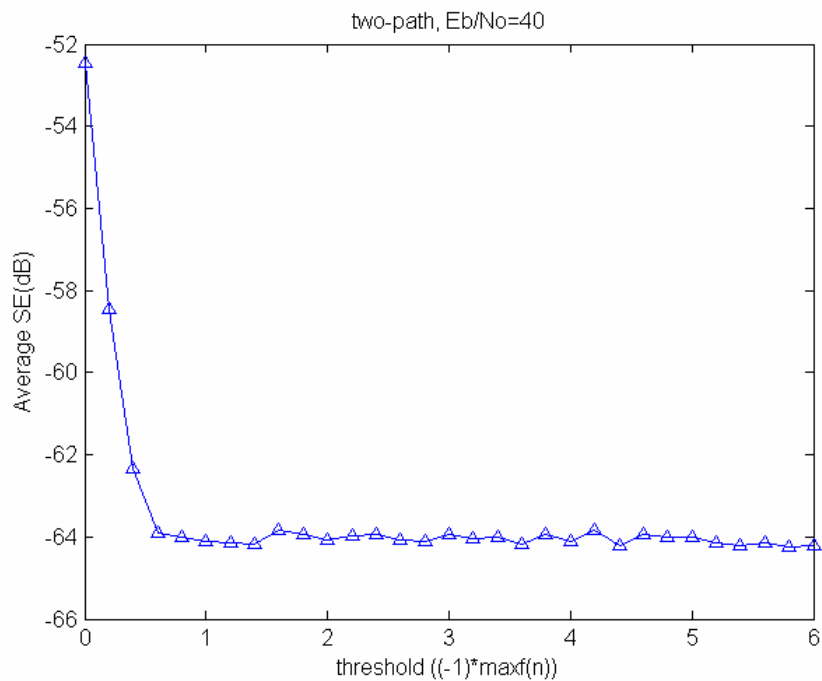


Figure 6.12 The average SE for the proposed path selection method in the two-path channel at  $E_b/N_0 = 40\text{dB}$  with threshold as a parameter.

## 6.2 System Performance in Veh. A

### Channel

In this section, we compare the performance of the three path selection methods in the ITU-Veh. A channel. For the number of path setting method, the parameter  $N_p$  is set as 64. For the threshold setting method, the parameter  $T_{dB}$  could be 20 or 30.

Figure 6.13 shows the BER performance for the three path selection methods. As shown in Figure 6.13, the threshold setting method with  $T_{dB} = 20$  experiences an error floor at  $\text{BER} = 8 \times 10^{-4}$ . Moreover, the threshold setting method with  $T_{dB} = 30$  performs almost the same as the proposed path selection method and the number of path setting method at the low  $E_b/N_0$  region, while it performs a little worse at the high  $E_b/N_0$  region. This implies that the BER performance for the threshold setting method is quite sensitive to the setting of the parameter  $T_{dB}$ .

Figure 6.14 shows the average SE for the three path selection methods. As can be seen in this figure, for the threshold setting method, both the parameters of  $T_{dB} = 20$  and  $T_{dB} = 30$  lead to an error floor due to the loss of channel paths. Besides, the average SE of the proposed method is about 10dB better than that of the number of path setting method for all  $E_b/N_0$  region.

Figure 6.15, Figure 6.17, and Figure 6.19 show the CDF of the false alarm for the three path selection methods at  $E_b/N_0 = 10\text{dB}$ ,  $25\text{dB}$ , and  $40\text{dB}$ , respectively. Figure 6.16, Figure 6.18, and Figure 6.20 show the CDF of the miss detection for the three path selection methods at  $E_b/N_0 = 10\text{dB}$ ,  $25\text{dB}$ , and  $40\text{dB}$ , respectively. We can find that the number of path setting method can exactly pick the six channel paths, but it also includes additional 58 fake paths. It should be noted that fake paths will increase the computation complexity of channel tracking. As can be seen in Figure 6.15, Figure 6.17, and Figure 6.19, we can observe that the threshold setting method with  $T_{dB} = 30$  has much higher false alarm probability at low  $E_b/N_0$ , as compared with the proposed method. For example, for the CDF=90% and  $E_b/N_0 = 10\text{dB}$ , the number of paths erroneously picked is 0 in the proposed method, while the number is 24 in the threshold setting method with  $T_{dB} = 30$ . This is because the threshold setting method picks noise as channel paths more easily at low  $E_b/N_0$ . Even though the threshold setting method with  $T_{dB} = 20$  has a little less number of paths erroneously picked than the proposed method, it suffers from severe degradation on the average SE and the BER performance. As shown in Figure 6.16, Figure 6.18, and Figure 6.20, we can observe that for the CDF of the miss detection at  $E_b/N_0 = 10\text{dB}$ , the threshold setting method with  $T_{dB} = 30$  performs a little better than the proposed method, whereas the threshold setting method with  $T_{dB} = 20$  performs much worse than the proposed method. Moreover, we can observe that the miss detection probability of the proposed



method is almost equal to 0 at  $E_b/N_0=25\text{dB}$  and  $40\text{dB}$ .

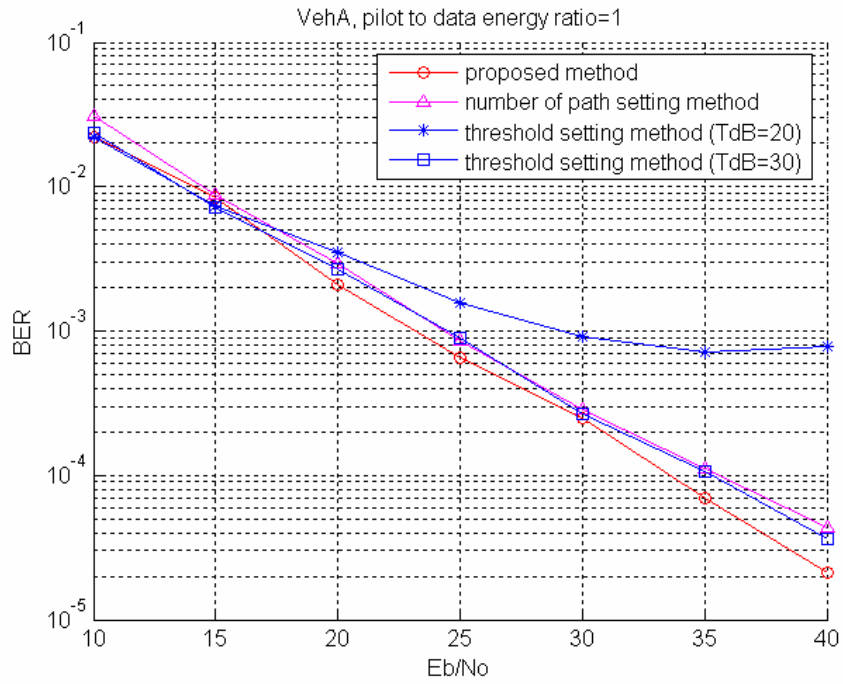


Figure 6.13 The BER performance for the three path selection methods in the Veh. A channel.

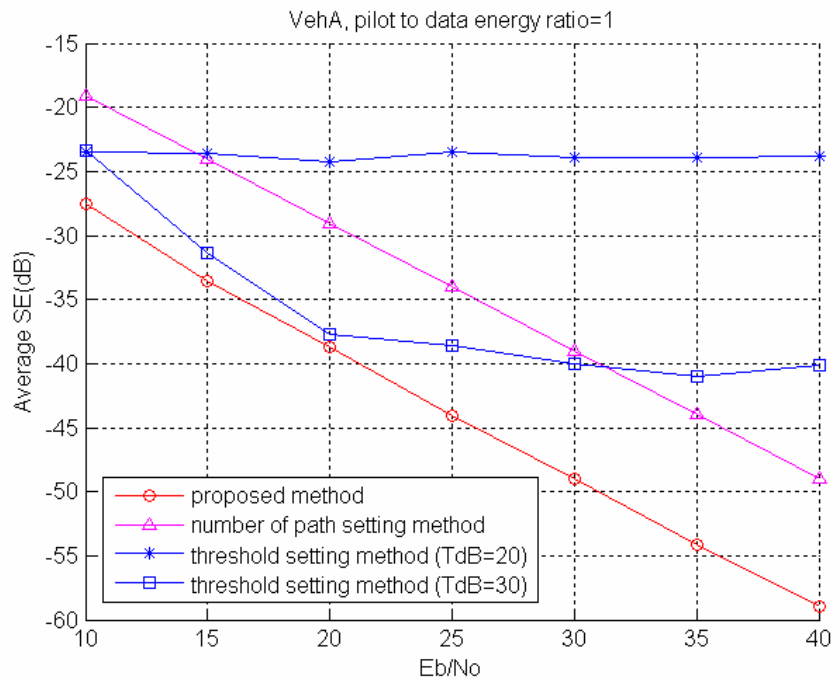


Figure 6.14 The average SE for the three path selection methods in the Veh. A channel.

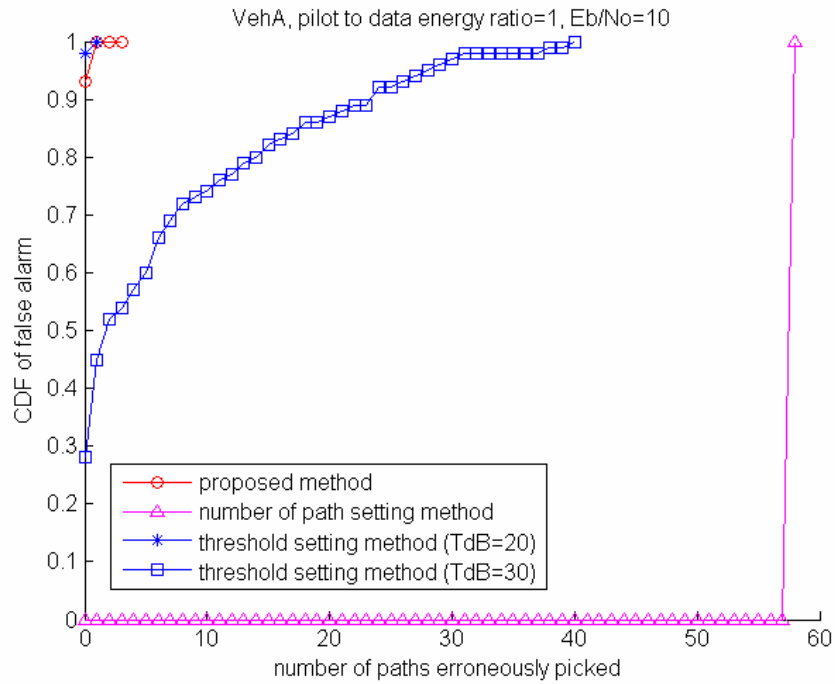


Figure 6.15 The CDF of false alarm for the three path selection methods at  $E_b/N_0 = 10\text{dB}$  in the Veh. A channel.

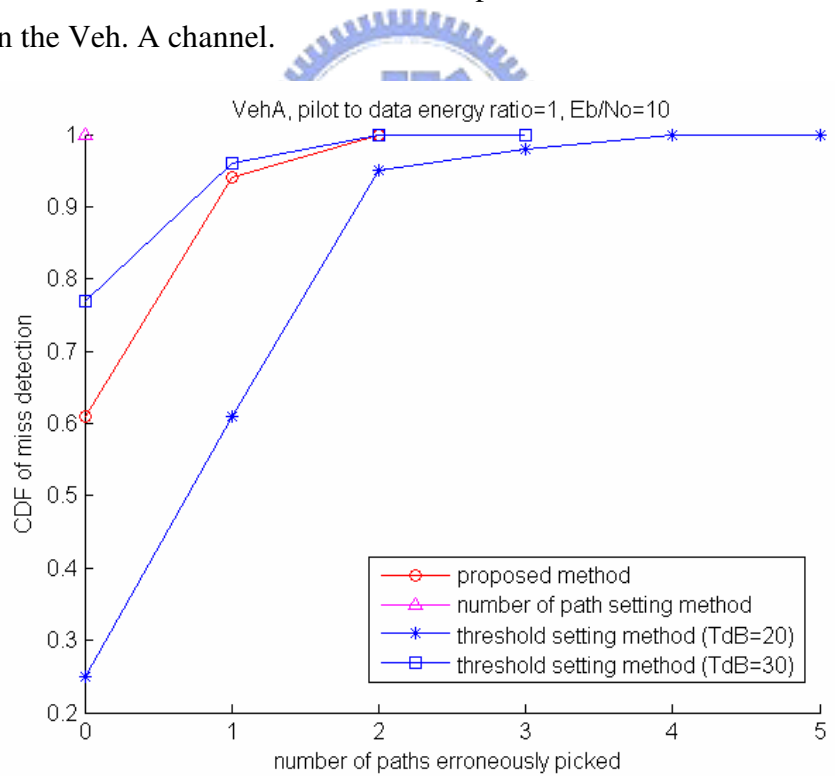


Figure 6.16 The CDF of miss detection for the three path selection methods at  $E_b/N_0 = 10\text{dB}$  in the Veh. A channel.

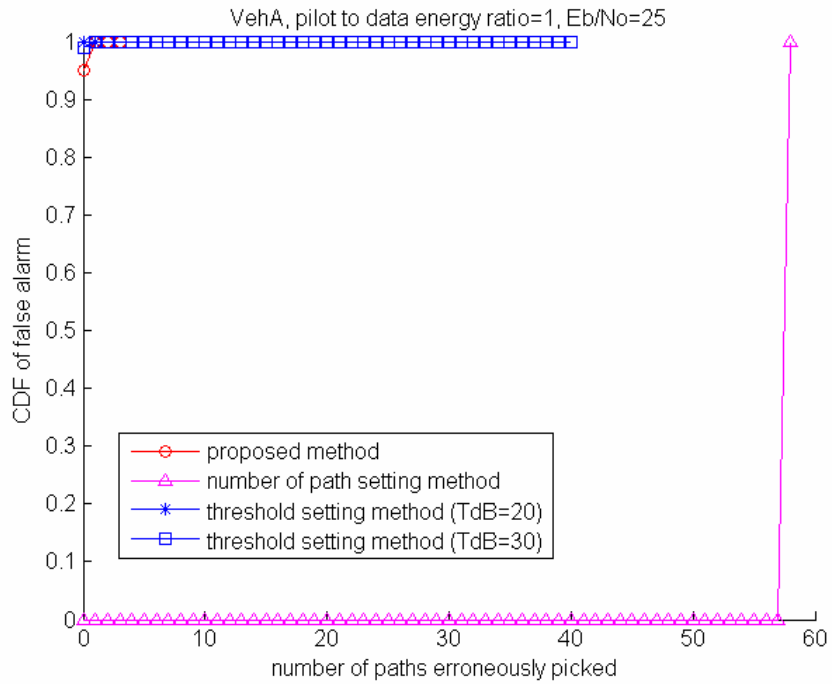


Figure 6.17 The CDF of false alarm for the three path selection methods at  $E_b/N_0 = 25\text{dB}$  in the Veh. A channel.

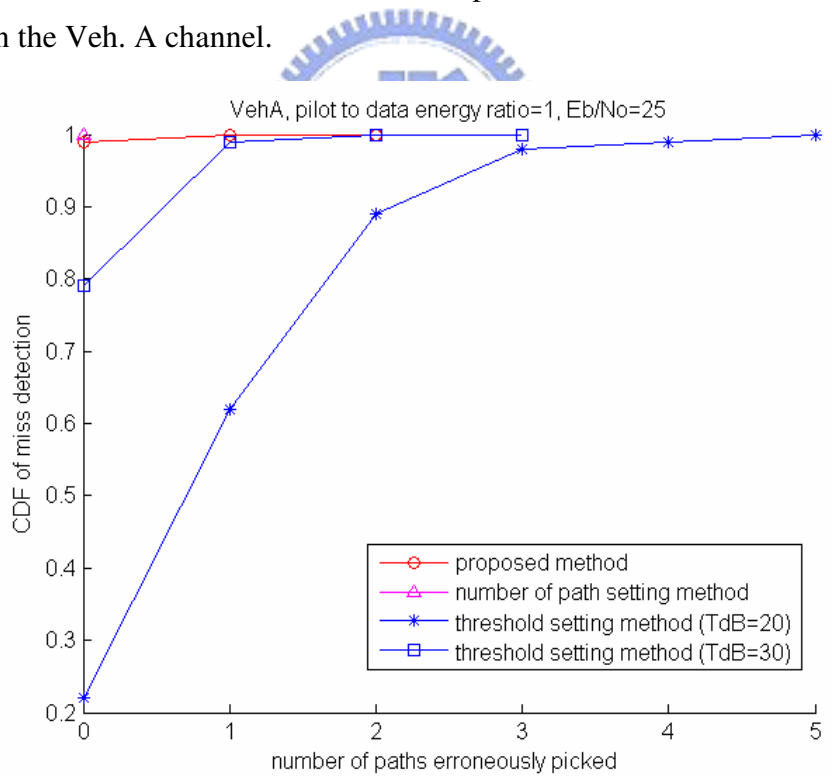


Figure 6.18 The CDF of miss detection for the three path selection methods at  $E_b/N_0 = 25\text{dB}$  in the Veh. A channel.

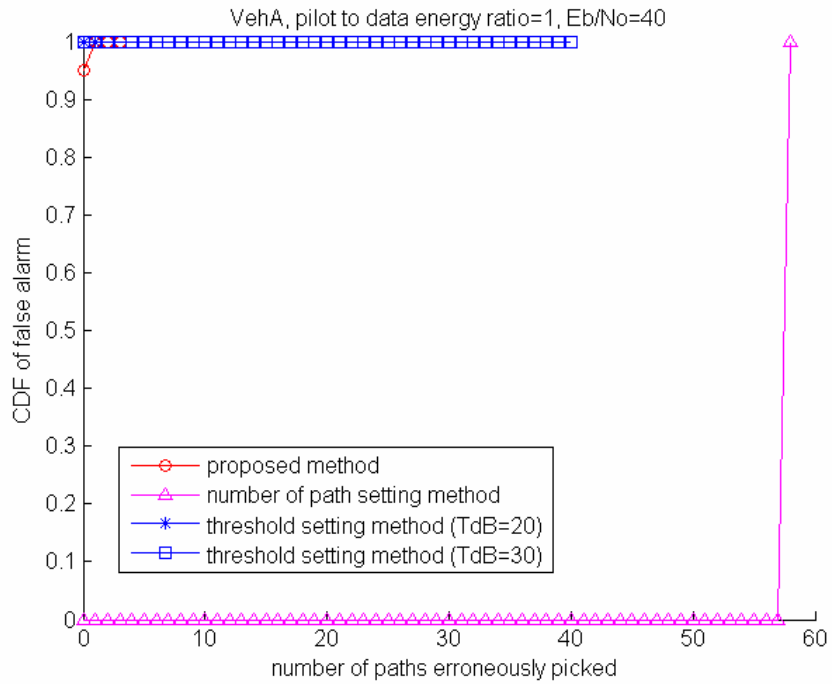


Figure 6.19 The CDF of false alarm for the three path selection methods at  $E_b/N_0 = 40\text{dB}$  in the Veh. A channel.

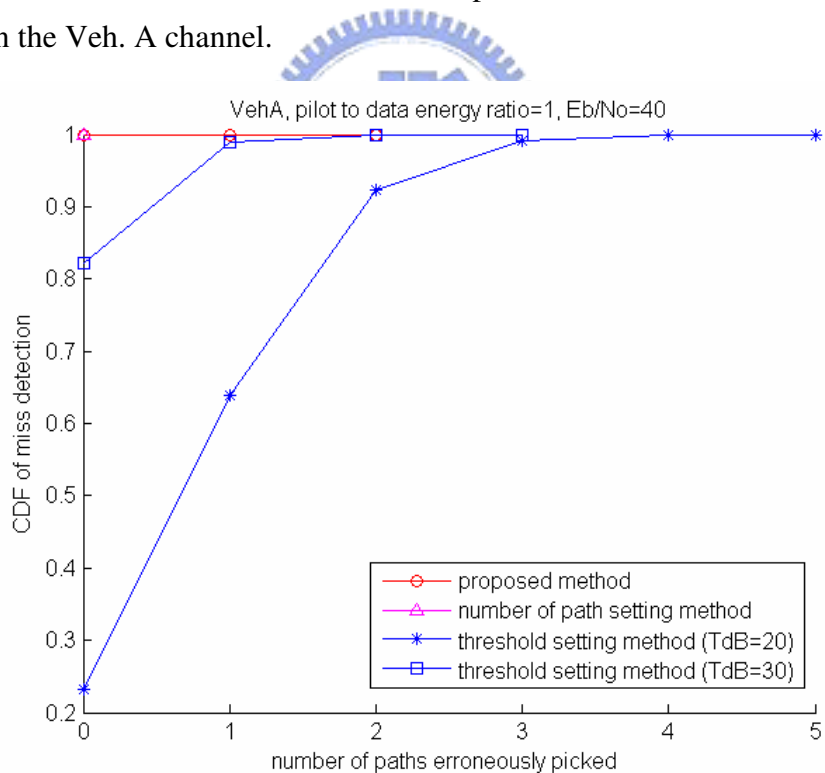


Figure 6.20 The CDF of miss detection for the three path selection methods at  $E_b/N_0 = 40\text{dB}$  in the Veh. A channel.

## 6.3 System Performance in Veh. B Channel

In this section, we compare the performance of the three path selection methods in the ITU-Veh. B channel. Figure 6.21 and Figure 6.22 show the BER and the average SE performance for the three path selection methods, respectively. Figure 6.23, Figure 6.25, and Figure 6.27 show the CDF of the false alarm for the three path selection methods at  $E_b/N_0=10\text{dB}$ ,  $25\text{dB}$ , and  $40\text{dB}$ , respectively. Figure 6.24, Figure 6.26, and Figure 6.28 show the CDF of the miss detection for the three path selection methods at  $E_b/N_0=10\text{dB}$ ,  $25\text{dB}$ , and  $40\text{dB}$ , respectively. According to these figures, we can observe that the simulation results obtained in the Veh. B channel are very similar to that in the Veh. A channel.

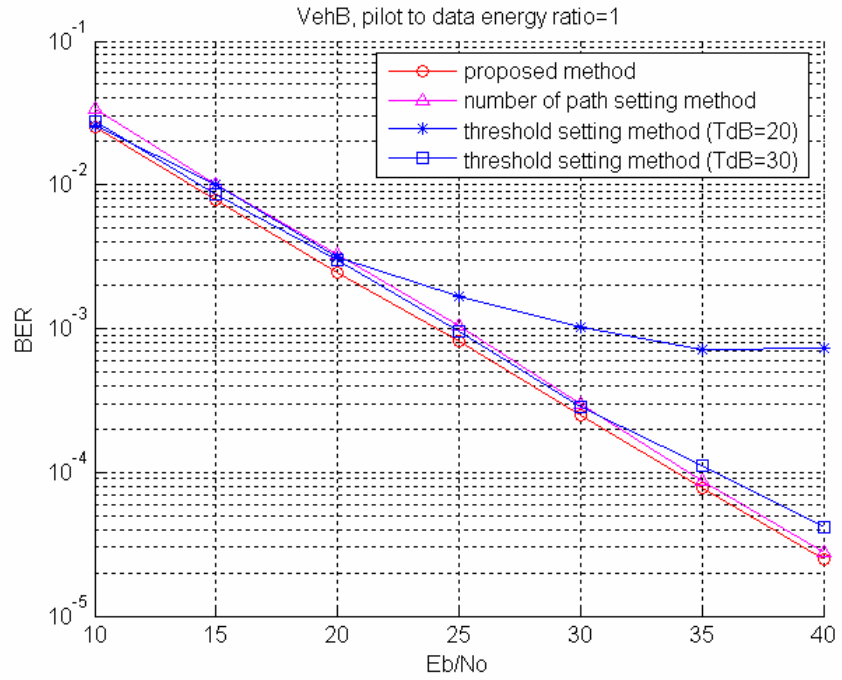


Figure 6.21 The BER performance for the three path selection methods in the Veh. B channel.

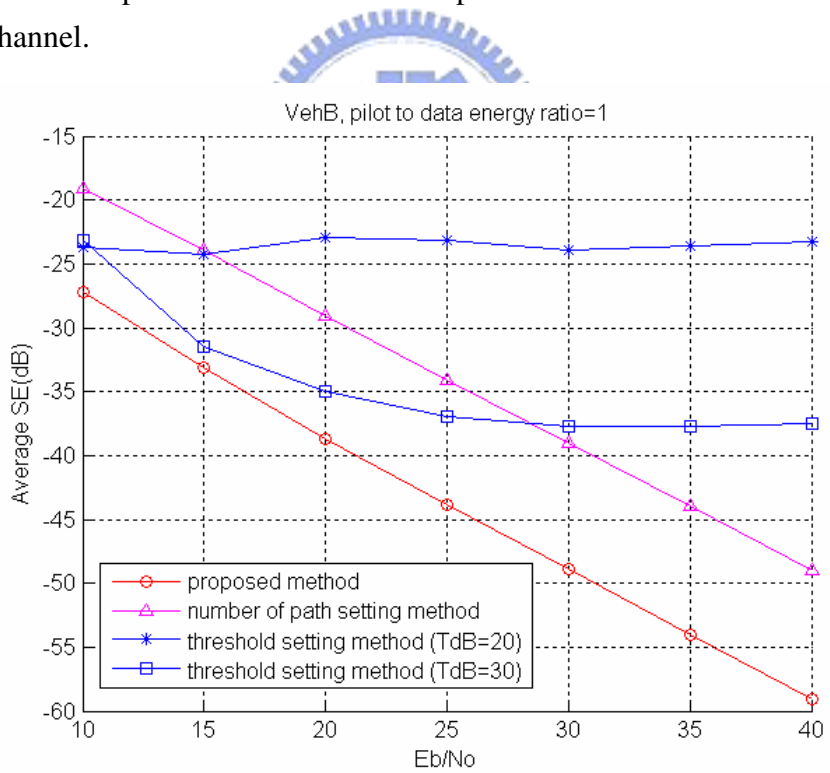


Figure 6.22 The average SE for the three path selection methods in the Veh. B channel.

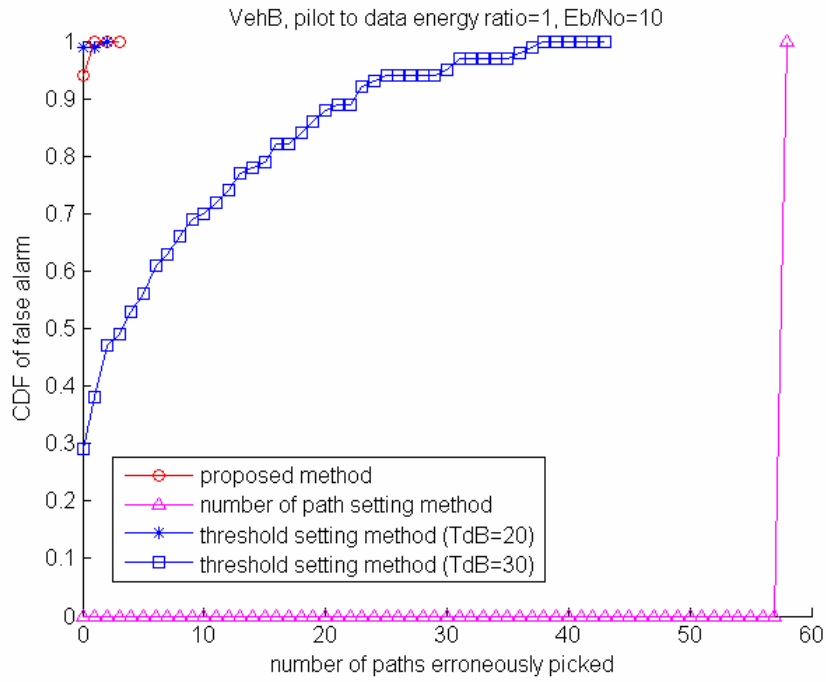


Figure 6.23 The CDF of false alarm for the three path selection methods at  $E_b/N_0 = 10\text{dB}$  in the Veh. B channel.

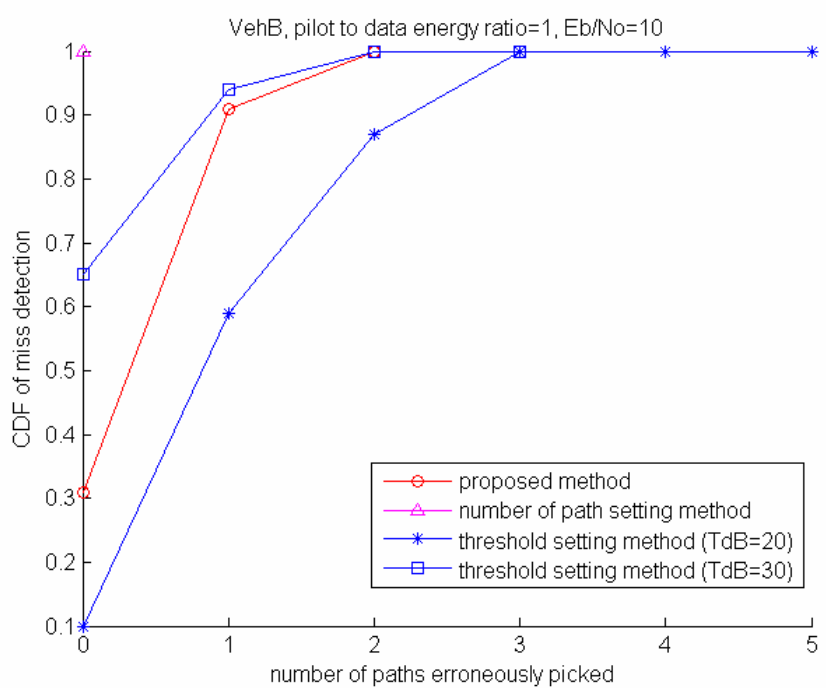


Figure 6.24 The CDF of miss detection for the three path selection methods at  $E_b/N_0 = 10\text{dB}$  in the Veh. B channel.

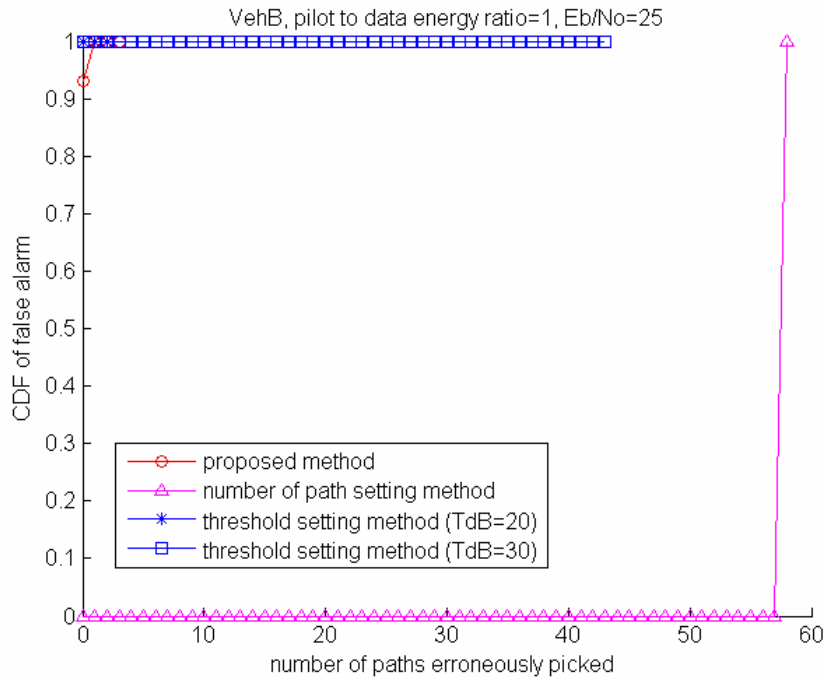


Figure 6.25 The CDF of false alarm for the three path selection methods at  $E_b/N_0 = 25\text{dB}$  in the Veh. B channel.

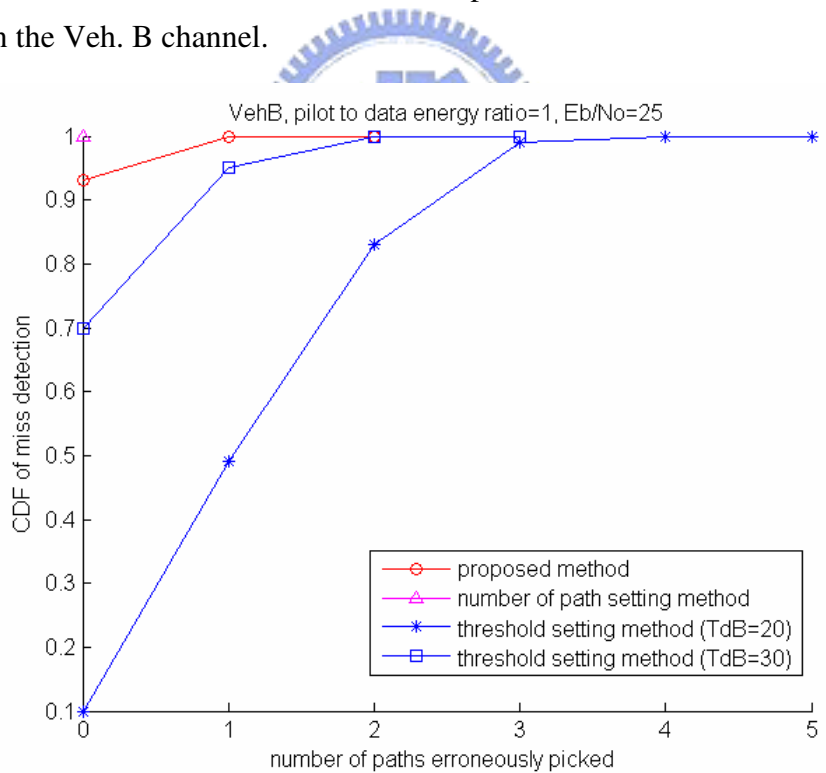


Figure 6.26 The CDF of miss detection for the three path selection methods at  $E_b/N_0 = 25\text{dB}$  in the Veh. B channel.



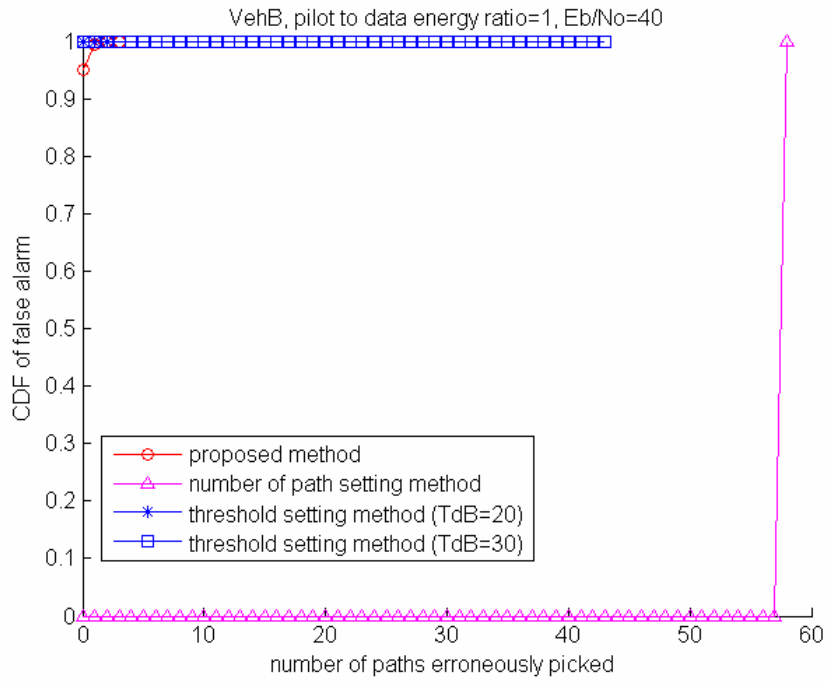


Figure 6.27 The CDF of false alarm for the three path selection methods at  $E_b/N_0 = 40\text{dB}$  in the Veh. B channel.

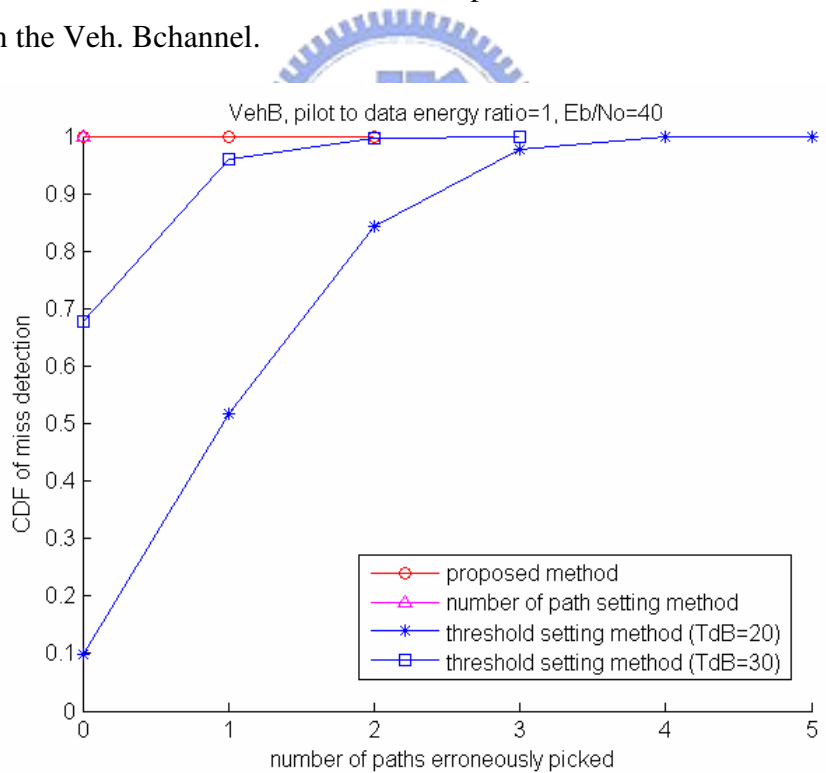


Figure 6.28 The CDF of miss detection for the three path selection methods at  $E_b/N_0 = 40\text{dB}$  in the Veh. B channel.

## 6.4 System Performance in two-path

### Channel

In this section, we compare the performance of the three path selection methods in the two-path channel. Figure 6.29 and Figure 6.30 show the BER and the average SE performance for the three path selection methods, respectively. As can be seen in Figure 6.30, at high  $E_b/N_0$  region, due to the fact that the energy of the two channel paths are much larger than noise energy, the average SE of the threshold setting method with  $T_{dB} = 30$  is a little larger than that of the proposed method, whereas the average SE of the threshold setting method with  $T_{dB} = 20$  experiences an floor and is larger than that of the proposed method. Therefore, the threshold setting method is still sensitive to the operating value of  $E_b/N_0$ . Moreover, the average SE of the proposed method is about 15dB lower than that of the number of path setting method. Figure 6.31, Figure 6.33, and Figure 6.35 show the CDF of the false alarm for the three path selection methods at  $E_b/N_0 = 10\text{dB}$ , 25dB, and 40dB, respectively. As can be seen in Figure 6.31, at CDF=99%, the threshold setting method with  $T_{dB} = 30$  performs much worse than the proposed method, and the threshold setting method with  $T_{dB} = 20$  is comparable to the proposed method. For the CDF of the false alarm at  $E_b/N_0 = 25\text{dB}$ , we can observe that the proposed method is slightly better than the threshold setting method with  $T_{dB} = 30$  at CDF=100%. Figure 6.32,

Figure 6.34, and Figure 6.36 show the CDF of the miss detection for the three path selection methods at  $E_b/N_0 = 10\text{dB}$ ,  $25\text{dB}$ , and  $40\text{dB}$ , respectively. As observed in these three figures, the miss detection probability (i.e., the value of the CDF when number of paths erroneously picked is zero) of the proposed method is equal to 0 and is a bit better than that of the threshold setting method.



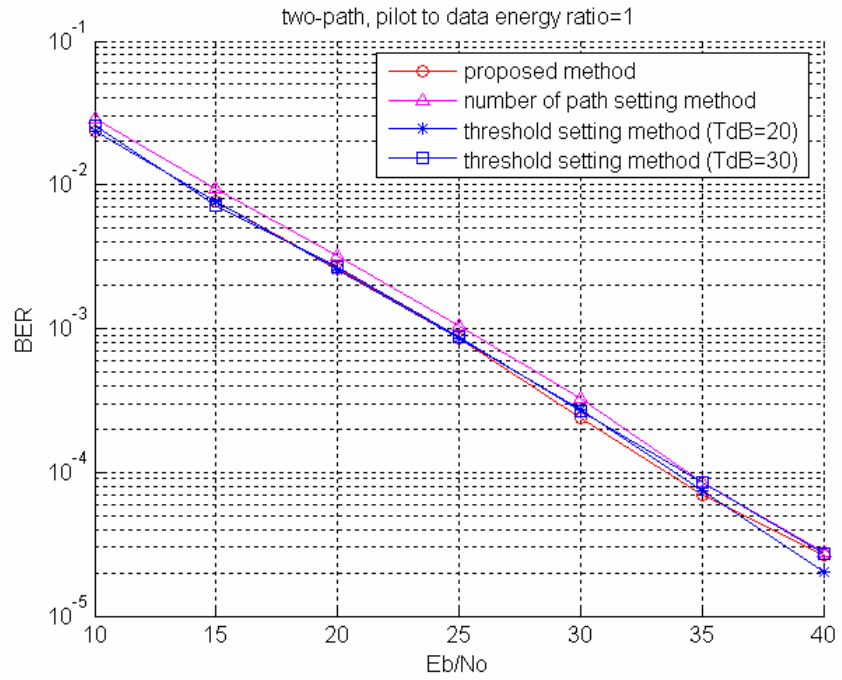


Figure 6.29 The BER performance for the three path selection methods in the two-path channel.

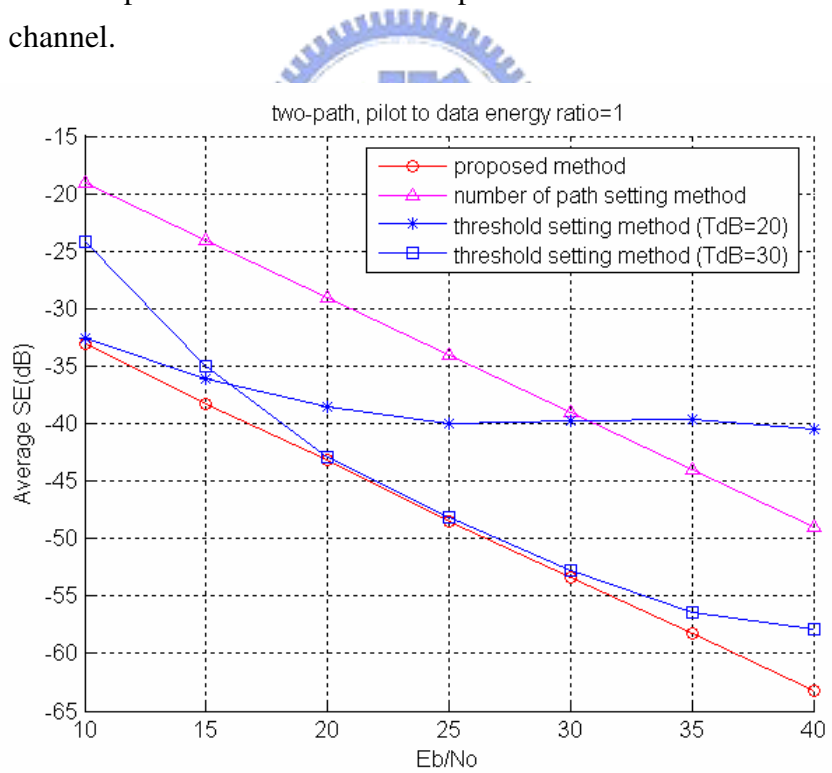


Figure 6.30 The average SE for the three path selection methods in the two-path channel.

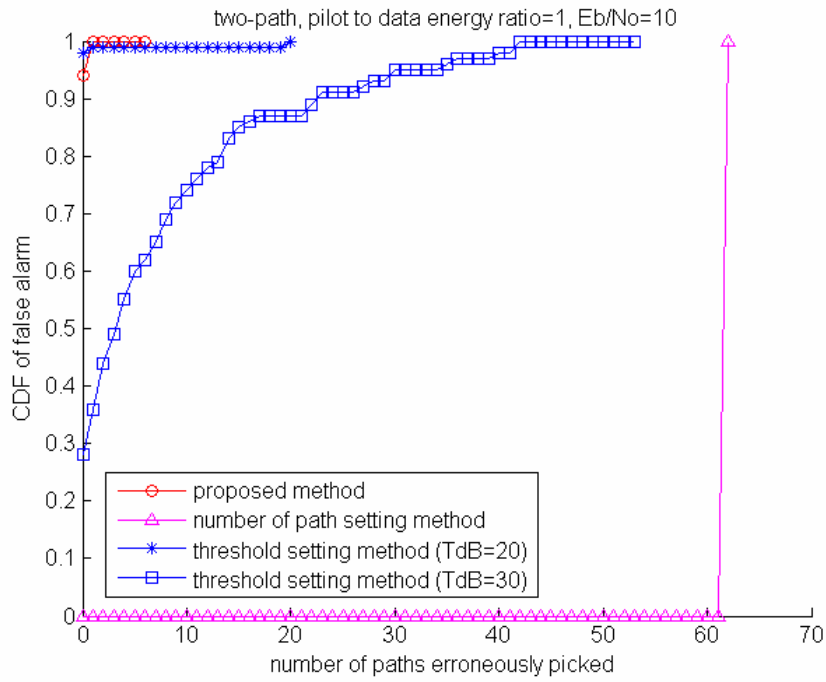


Figure 6.31 The CDF of the false alarm for the three path selection methods at  $E_b/N_0 = 10\text{dB}$  in the two-path channel.

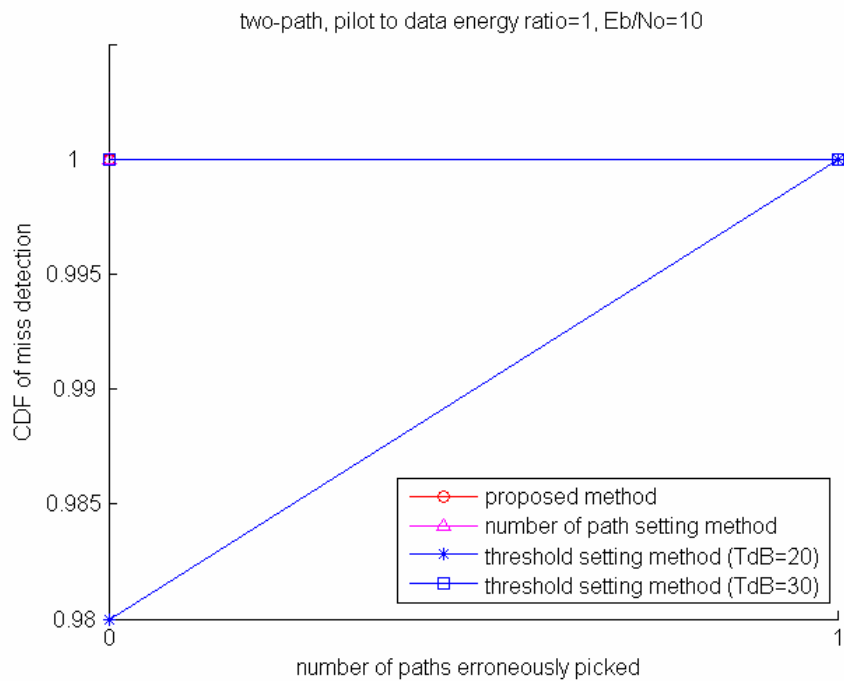


Figure 6.32 The CDF of miss detection for the three path selection methods at  $E_b/N_0 = 10\text{dB}$  in the two-path channel.

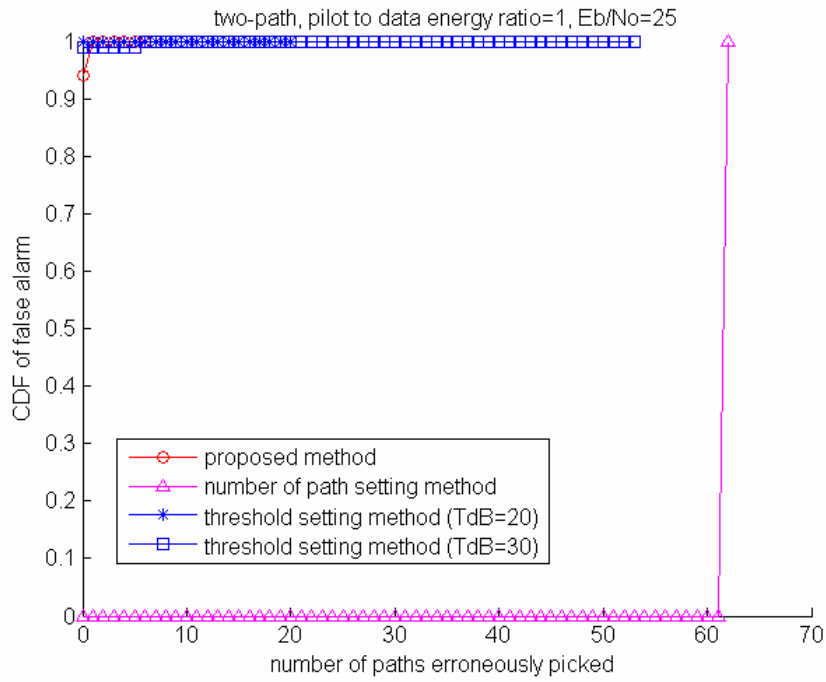


Figure 6.33 The CDF of the false alarm for the three path selection methods at  $E_b/N_0 = 25\text{dB}$  in the two-path channel.

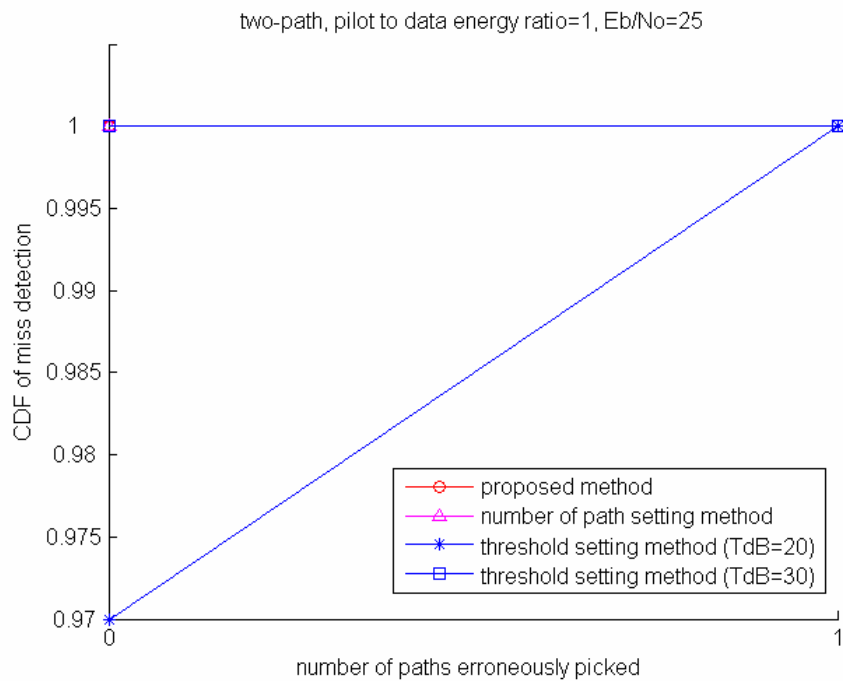


Figure 6.34 The CDF of miss detection for the three path selection methods at  $E_b/N_0 = 25\text{dB}$  in the two-path channel.

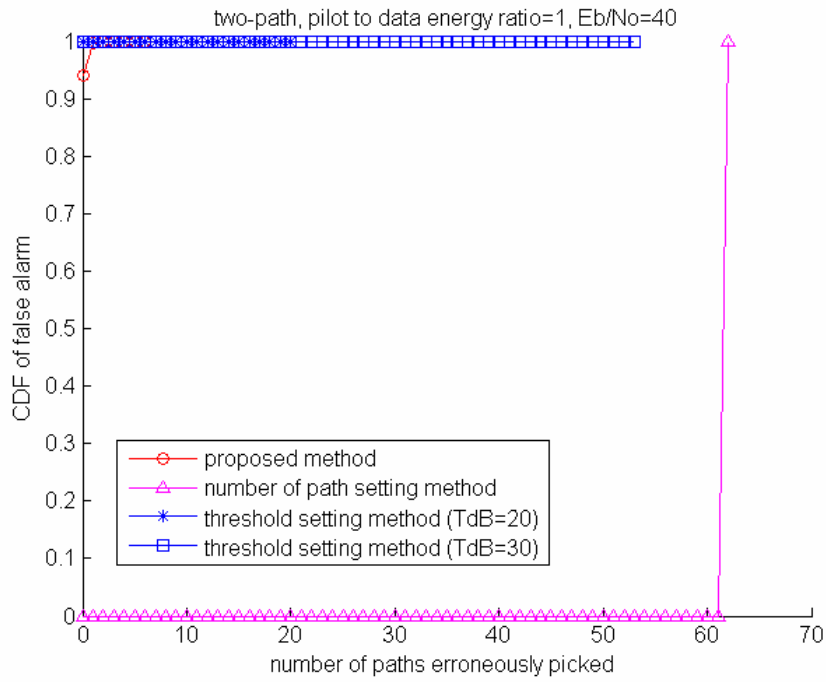


Figure 6.35 The CDF of the false alarm for the three path selection methods at  $E_b/N_0 = 40\text{dB}$  in the two-path channel.

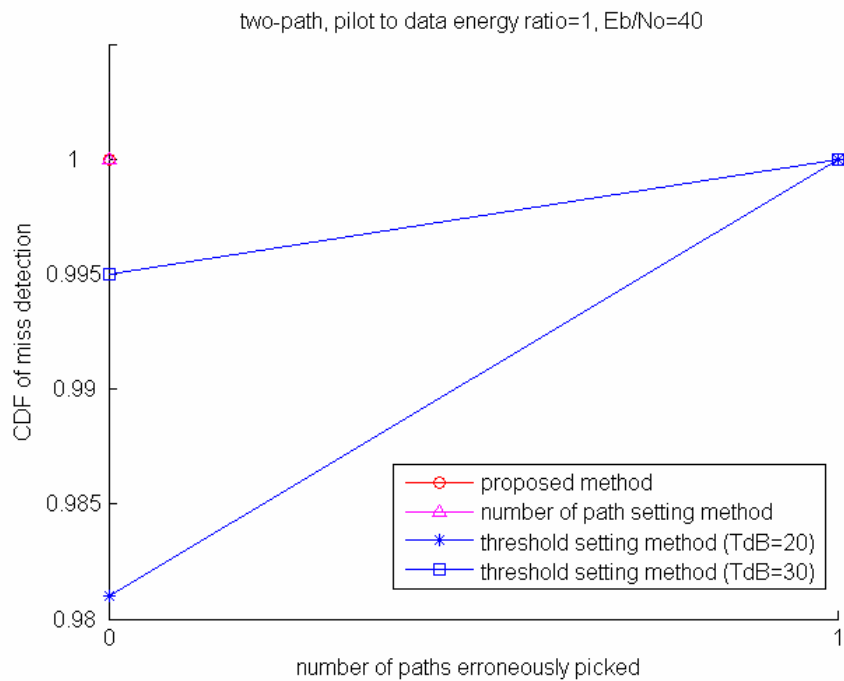


Figure 6.36 The CDF of miss detection for the three path selection methods at  $E_b/N_0 = 40\text{dB}$  in the two-path channel.

## 6.5 System Performance in thirty-path Channel

In this section, we simulate the performance of the three path selection methods in the thirty-path exponentially decaying channel in which the decaying factor is set as  $\beta = 0.3$ .

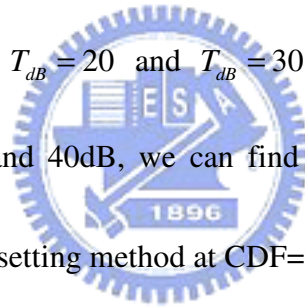
Figure 6.37 and Figure 6.38 show the BER and the average SE performance for the three path selection methods, respectively. As shown in Figure 6.37, since the channel paths with smaller energy are discarded, an error floor is clearly visible at  $\text{BER} = 5 \times 10^{-3}$  and  $\text{BER} = 5 \times 10^{-4}$  for the threshold setting method with  $T_{dB} = 20$  and  $T_{dB} = 30$ , respectively. We can also observe that in Figure 6.38, whether the threshold  $T_{dB}$  is 20 or 30, no improvement in the average SE of the threshold setting method can be achieved when  $E_b/N_0$  is larger than 25dB. We can further observe that the BER performance of the proposed method performs slightly better than that of the number of path setting method, and the average SE performance of the proposed method is about 2dB better than that of the number of path setting method.

Figure 6.39, Figure 6.41, and Figure 6.43 show the CDF of the false alarm for the three path selection methods at  $E_b/N_0 = 10\text{dB}$ ,  $25\text{dB}$ , and  $40\text{dB}$ , respectively. From these three figures, we can find that the proposed method and the threshold setting method with



$T_{dB} = 20$  is better than the threshold setting method with. For example, at  $E_b/N_0 = 10\text{dB}$  and  $\text{CDF} = 100\%$ , the number of paths erroneously picked by the proposed method and the threshold setting method with  $T_{dB} = 20$  is 0, and the number is less than 30 incorrect paths for the threshold setting method with  $T_{dB} = 30$ .

Figure 6.40, Figure 6.42 and Figure 6.44 show the CDF of the miss detection for the three path selection methods at  $E_b/N_0 = 10\text{dB}$ ,  $25\text{dB}$ , and  $40\text{dB}$ , respectively. We can notice that for  $E_b/N_0 = 10\text{dB}$  and  $\text{CDF} = 90\%$ , the number of paths erroneously picked by the proposed method is less than 14, while the number of paths erroneously picked by the threshold setting method with  $T_{dB} = 20$  and  $T_{dB} = 30$  is less than 18 and 9, respectively. However, for  $E_b/N_0 = 25\text{dB}$  and  $40\text{dB}$ , we can find that the proposed method performs much better than the threshold setting method at  $\text{CDF} = 90\%$ .



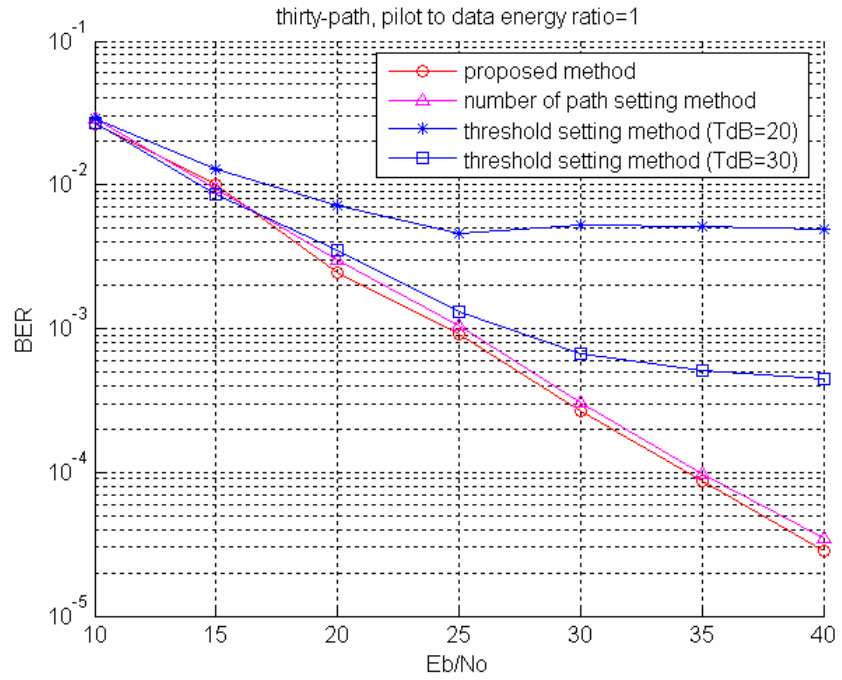


Figure 6.37 The BER performance for the three path selection methods in the thirty-path channel.

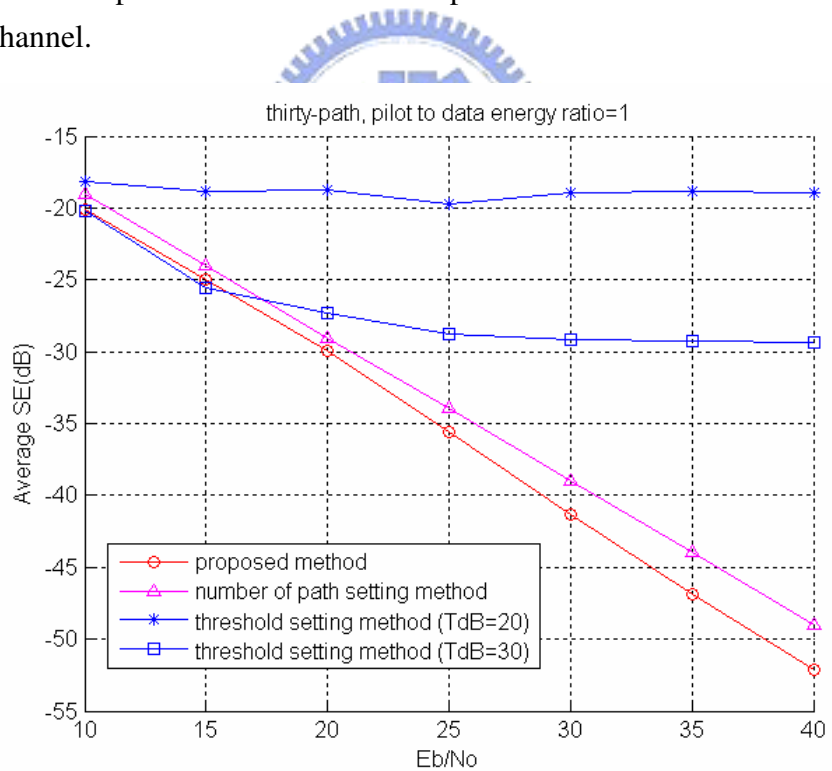


Figure 6.38 The average SE performance for the three path selection methods in the thirty-path channel.

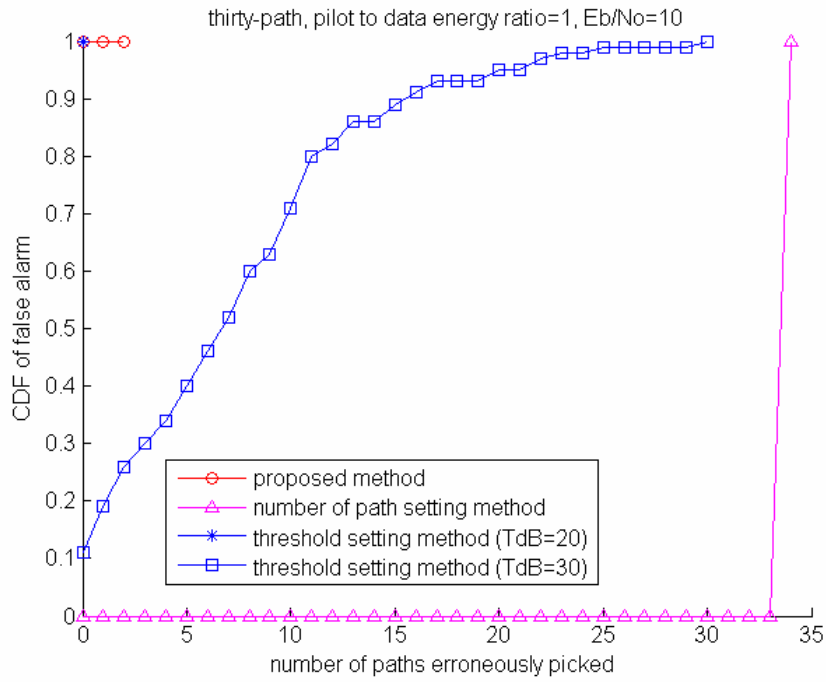


Figure 6.39 The CDF of false alarm for the three path selection methods at  $E_b/N_0 = 10\text{dB}$  in the thirty-path channel.

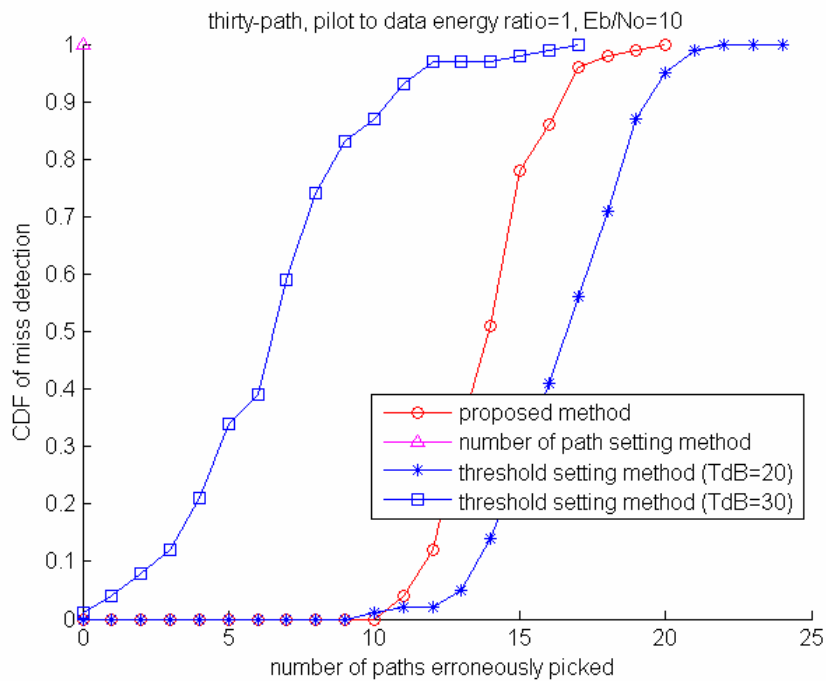


Figure 6.40 The CDF of miss detection for the three path selection methods at  $E_b/N_0 = 10\text{dB}$  in the thirty-path channel.

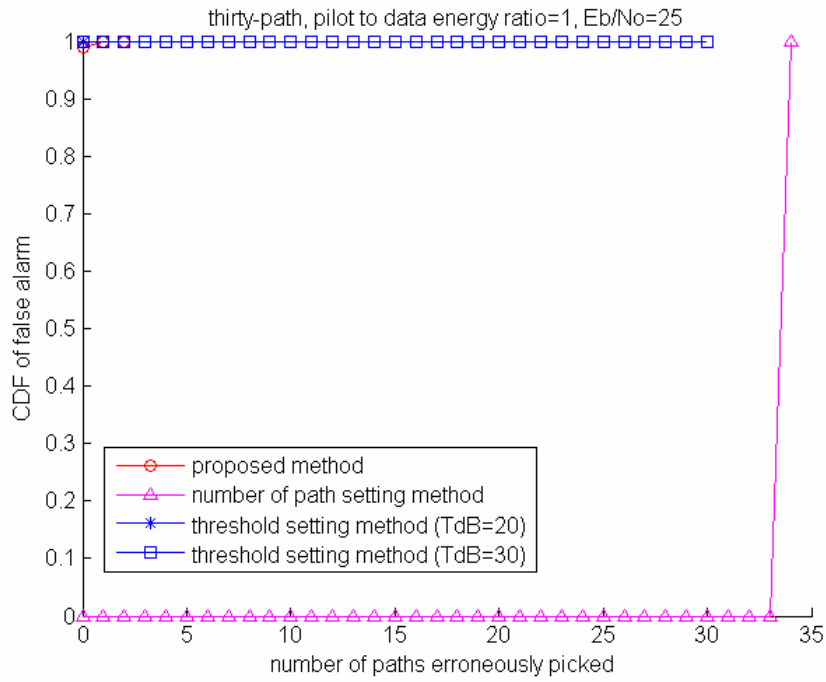


Figure 6.41 The CDF of false alarm for the three path selection methods at  $E_b/N_0 = 25\text{dB}$  in the thirty-path channel.

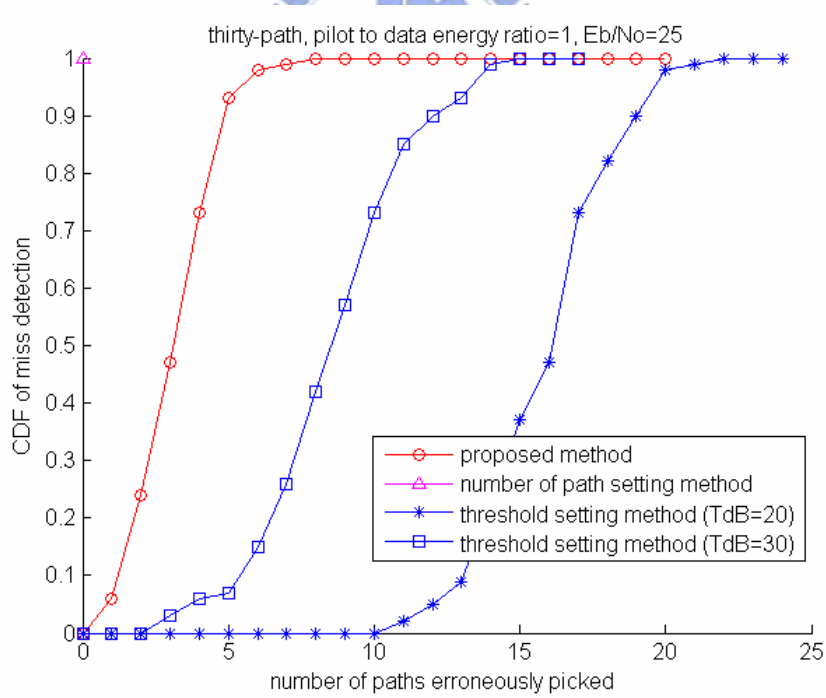


Figure 6.42 The CDF of miss detection for the three path selection methods at  $E_b/N_0 = 25\text{dB}$  in the thirty-path channel.

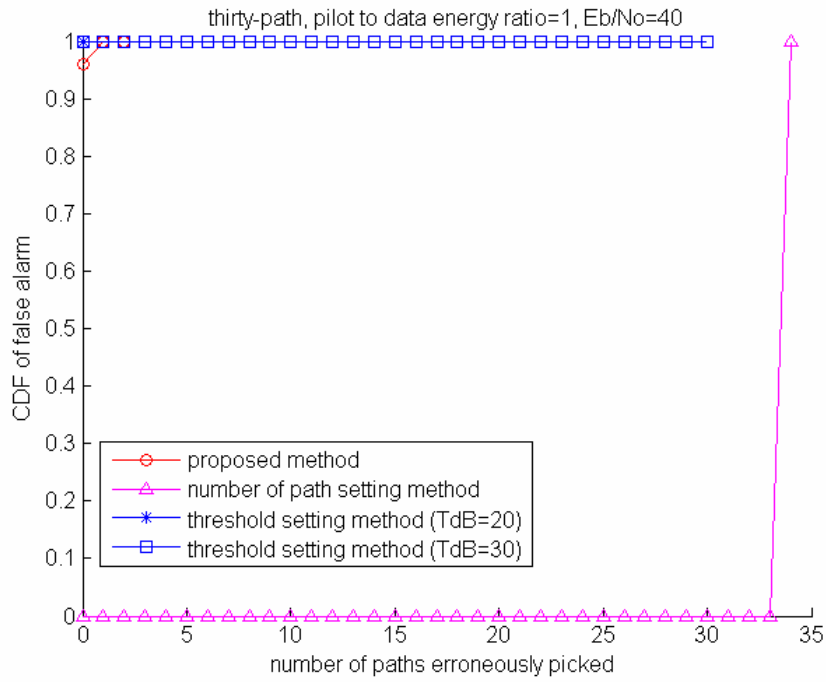


Figure 6.43 The CDF of false alarm for the three path selection methods at  $E_b/N_0 = 40\text{dB}$  in the thirty-path channel.

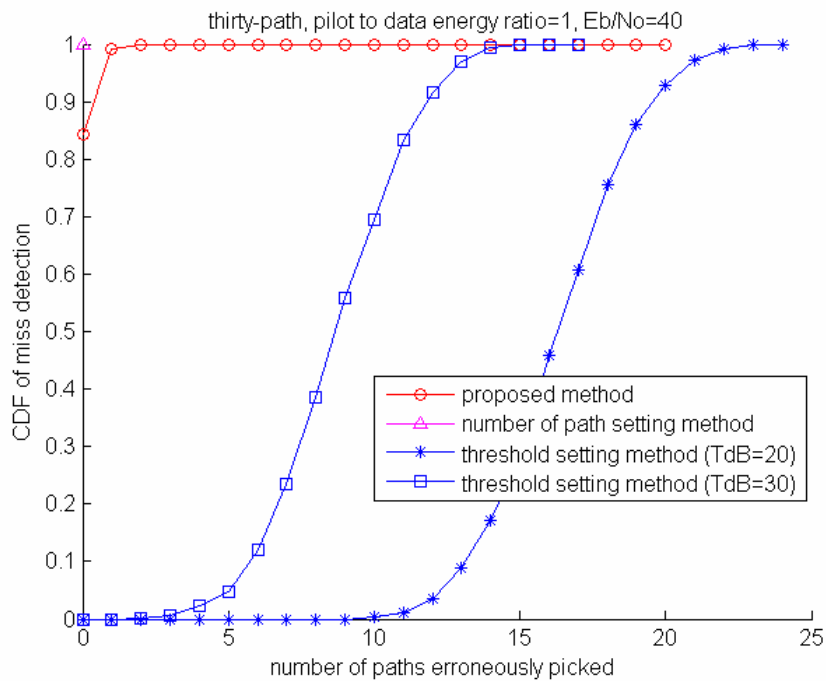
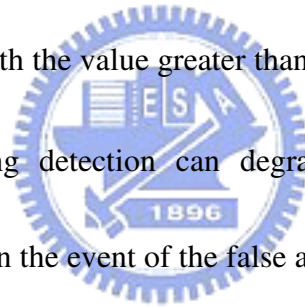


Figure 6.44 The CDF of miss detection for the three path selection methods at  $E_b/N_0 = 40\text{dB}$  in the thirty-path channel.

## 6.5.1 System Performance of Number of Path Setting Method with Different $N_p$

Computer simulations are carried out in the thirty-path exponentially decayed channel to examine the performance of the number of path setting method under different values of  $N_p$ . Here, the values of  $N_p$  could be 10, 20, 30, 40, 50, and 60. Figure 6.45 and Figure 6.46 show the BER and the average SE performance for the number of path setting method with  $N_p$  as a parameter, respectively. Figure 6.45 and Figure 6.46 show that  $N_p$  with the value less than 30 (number of channel paths existing in channel environment) causes much more degradation than  $N_p$  with the value greater than or equal to 30. This result concludes that the event of the missing detection can degrade the BER and the average SE performance more severely than the event of the false alarm.



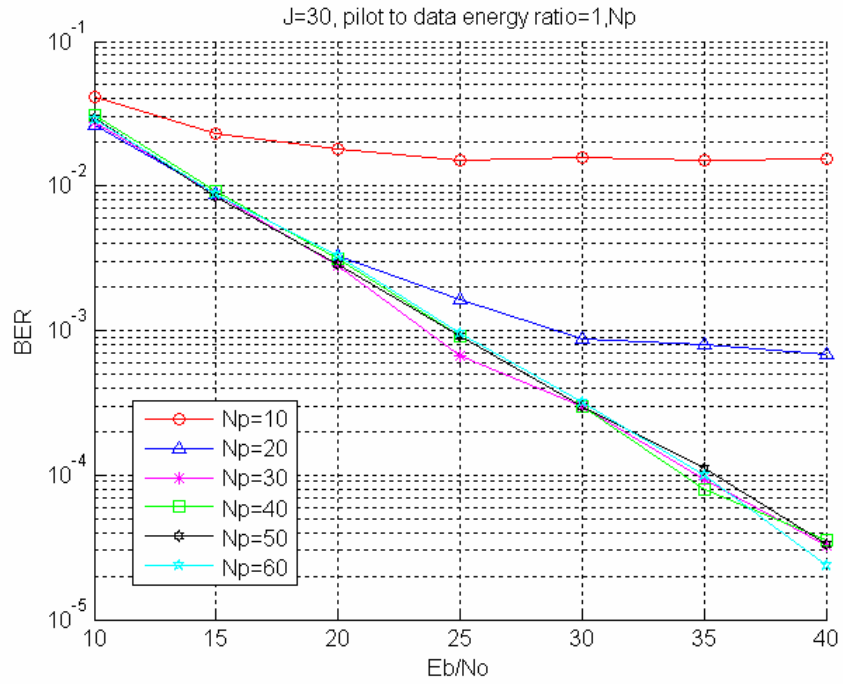


Figure 6.45 The BER performance for the number of path setting method with  $N_p$  as a parameter in the thirty-path channel.

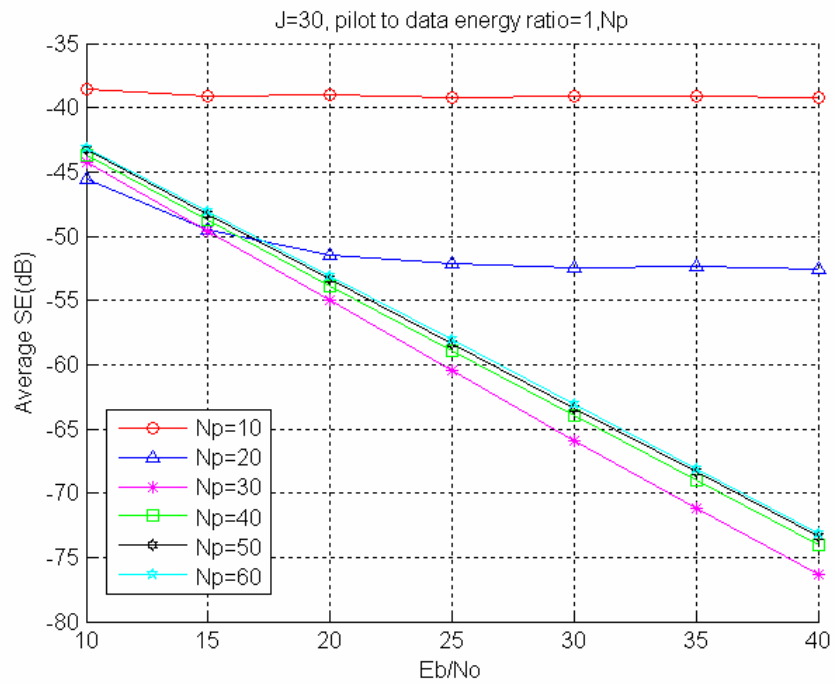


Figure 6.46 The average SE for the number of path setting method with  $N_p$  as a parameter in the thirty-path channel.

# Chapter 7

## Conclusions

DFT-based channel estimation which is derived from either ML or MMSE criterion was intensively investigated for PA channel estimation in OFDM systems. Several kinds of path selection methods are used to suppress noise and to further improve the performance of channel estimation. After the path selection, the estimated channel impulse response is transformed back into frequency-domain to obtain the estimated channel frequency response.



However, the conventional path selection methods require knowledge of the multi-path power delay profile, the number of channel taps, and the operating SNR. If such knowledge is not available, the performance of channel estimation may be degraded severely.

In this thesis, we propose a novel path selection method for channel estimation in OFDM systems. First, the cost function of the proposed method can be formulated as an integer linear programming problem. We then find that the ILP problem can be minimized by using a simple sorting problem. We further refine the proposed algorithm by analyzing the event of false alarm and set a new threshold for the algorithm.

We compare the performances of our proposed method with the two conventional



methods by using computer simulation. Comparing to the conventional methods, the simulation results show that the proposed method can improve BER performance, reduce average SE of channel estimation, and increase the probability of picking channel paths. Finally, the simulation results also show that our proposed method is insensitive to the multi-path power delay profile as well as the operating SNR.



# Bibliography

- [1] L. Deneire, P. Vandenameele, L. van der Perre, B. Gyselinckx and M. Engels, "A Low-Complexity ML Channel Estimator for OFDM," *IEEE Trans. Commun.*, vol. 51, no. 2, pp. 135 – 140, Feb. 2003.
- [2] M. Morelli and U. Mengali, "A comparison of pilot-aided channel estimation methods for OFDM systems," *IEEE Trans. Signal Processing*, vol. 49, no. 12, pp. 3065 – 3073, Dec. 2001.
- [3] G. L. Stuber, J. R. Barry, S. W. McLaughlin, Ye Li, M. A. Ingram and T. G. Pratt, "Broadband MIMO-OFDM wireless communications," *Proceedings of the IEEE*, vol. 92, no. 2, pp. 271 – 294, Feb. 2004.
- [4] J. G. Proakis, "Digital Communications," *McGraw-Hill*, 4th edition, 2000.
- [5] O. Edfors, M. Sandell, J.-J. van de Beek, S. K. Wilson and P. O. Borjesson, "Analysis of DFT-based channel estimators for OFDM," in *Personal Wireless Commun.* vol. 12, Jan. 2000.
- [6] Shin-Yuan Wang and Chia-Chi Huang, "On the architecture and performance of an FFT-based spread-spectrum downlink RAKE receiver," *IEEE Trans. Veh. Technol.*, vol. 50, no. 1, pp. 234 – 243, Jan. 2001.
- [7] Meng-Lin Ku and Chia-Chi Huang, "A Complementary Codes Pilot-Based Transmitter Diversity Technique for OFDM Systems," *IEEE Trans. Wireless Commun*, vol. 5, no. 3, pp. 504 – 508, March 2006.
- [8] O. Edfors, M. Sandell, J.J. van de Beek, D. Landstrom and F. Sjoberg, "An introduction to orthogonal frequency division multiplexing," Lulea University of Technology, Sep. 1996.
- [9] Richard van Nee and Ramjee Prasad, "OFDM wireless multimedia communications," *Artech House*, 2000.
- [10] Jasbir S. Arora, "Introduction to optimum design," *Elsevier Academic press*, 2004.
- [11] Christian P. Robert and George Casella, "Monte-Carlo statistical methods," *Springer*, 2nd edition, 2004.
- [12] T. B. Sørensen, P. E. Mogensen and F. Frederiksen, "Extension of the ITU Channel Models for Wideband (OFDM) Systems," *IEEE Conf. Veh. Technol.*, vol. 1, pp. 392 – 396, 2005.
- [13] Tiejun Wang, John G. Proakis, and James R. Zeidler, "Techniques for suppression of intercarrier interference in OFDM systems," *IEEE Conf. Wireless Commun. and*

*Networking*, vol. 1, pp. 39 – 44, March 2005.



